

Complex-Temperature Properties of the 2D Ising Model with $\beta H = \pm i\pi/2$

Victor Matveev* and Robert Shrock**

Institute for Theoretical Physics
State University of New York
Stony Brook, N. Y. 11794-3840

Abstract

We study the complex-temperature properties of a rare example of a statistical mechanical model which is exactly solvable in an external symmetry-breaking field, namely, the Ising model on the square lattice with $\beta H = \pm i\pi/2$. This model was solved by Lee and Yang [1]. We first determine the complex-temperature phases and their boundaries. From a low-temperature, high-field series expansion of the partition function, we extract the low-temperature series for the susceptibility χ to $O(u^{23})$, where $u = e^{-4K}$. Analysing this series, we conclude that χ has divergent singularities (i) at $u = u_e = -(3 - 2^{3/2})$ with exponent $\gamma'_e = 5/4$, (ii) at $u = 1$, with exponent $\gamma'_1 = 5/2$, and (iii) at $u = u_s = -1$, with exponent $\gamma'_s = 1$. We also extract a shorter series for the staggered susceptibility and investigate its singularities. Using the exact result of Lee and Yang for the free energy, we calculate the specific heat and determine its complex-temperature singularities. We also carry this out for the uniform and staggered magnetisation.

*email: vmatveev@max.physics.sunysb.edu

**email: shrock@max.physics.sunysb.edu

1 Introduction

The Ising model has long served as a prototype of a statistical mechanical system which undergoes a phase transition with associated spontaneous symmetry breaking and long range order. In the absence of an external magnetic field H , the free energy of the $d = 2$ (spin 1/2) Ising model was first calculated by Onsager [2], and the expression for the spontaneous magnetisation first calculated by Yang [3], both for the square lattice. The model has never been solved in an arbitrary external magnetic field. However, in one of their classic papers, Lee and Yang [1] did succeed in solving exactly for the free energy and giving an exact expression for the magnetisation of the Ising model on the square lattice for a particular manifold of values of H depending on the temperature T , given by

$$H = \frac{i\pi k_B T}{2} \tag{1.1}$$

Although this is not a physical set of values, owing to the imaginary value of H and the resultant non-hermiticity of the Hamiltonian, this model is nevertheless of considerable interest as a rare example of a statistical mechanical model for which one has an exact solution in the presence of a symmetry-breaking field. Further work on the derivation of the Lee-Yang solution was reported in Refs. [4, 5, 6, 7].

In the present paper, we shall investigate this model in a wider context, generalising the temperature to complex values. There are several reasons for studying the properties of statistical mechanical systems with the temperature variable generalised to take on complex values. First, one can understand more deeply the behaviour of various thermodynamic quantities by seeing how they behave as analytic functions of complex temperature. Second, one can see how the physical phases of a given model generalise to regions in appropriate complex-temperature variables. Third, a knowledge of the complex-temperature singularities of quantities which have not been calculated exactly helps in the search for exact, closed-form expressions for these quantities. This applies, in particular, to the susceptibility of the present model, which, like that of the zero-field Ising model, has never been calculated.

2 Generalities and Complex-Temperature Phases

In this section we shall work out the complex-temperature phases and their boundaries. We begin with some definitions and notation. Recall that the Ising model is defined by the partition function $Z = \sum_{\{\sigma_n\}} e^{-\beta\mathcal{H}}$ with the Hamiltonian

$$\mathcal{H} = -J \sum_{\langle nn' \rangle} \sigma_n \sigma_{n'} - H \sum_n \sigma_n \tag{2.1}$$

where $\sigma_n = \pm 1$ are the Z_2 spin variables on each site n of the lattice, $\beta = (k_B T)^{-1}$, J is the exchange constant, $\langle nn' \rangle$ denote nearest-neighbor pairs, and the units are defined such that the magnetic moment which would multiply the $H \sum_n \sigma_n$ is unity. We shall concentrate here on the square (sq) lattice. We use the standard notation $K = \beta J$, $h = \beta H$, $v = \tanh K$, $z = e^{-2K}$, $u = z^2 = e^{-4K}$, $w = 1/u$, and $\mu = e^{-2h}$. Note that v and z are related by the bilinear conformal transformation

$$z = \frac{1-v}{1+v} \quad (2.2)$$

It will also be useful to introduce two elliptic moduli. The first is

$$\kappa = \frac{1}{C^2} = \frac{4u}{(1+u)^2} \quad (2.3)$$

which occurs in elliptic integrals in the exact expressions for the internal energy and specific heat, where we use the abbreviations

$$C \equiv \cosh(2K) \quad (2.4)$$

$$S \equiv \sinh(2K) \quad (2.5)$$

We record the symmetry

$$u \rightarrow 1/u \quad \Rightarrow \quad \kappa \rightarrow \kappa \quad (2.6)$$

The second elliptic modulus,

$$k_{<} = \frac{i}{S(S^2+2)^{1/2}} = \frac{4iu}{(1-u)(1+6u+u^2)^{1/2}} \quad (2.7)$$

occurs in a natural way in the magnetisation.¹

The reduced free energy per site is $f = -\beta F = \lim_{N_s \rightarrow \infty} N_s^{-1} \ln Z$ (where N_s denotes the number of sites on the lattice). In addition to the susceptibility itself, it will also be convenient to refer to the reduced susceptibility $\bar{\chi} = \beta^{-1} \chi$.

We begin by discussing the phase boundaries of the model as a function of complex temperature, i.e. the locus of points across which the free energy is non-analytic. As noted in Ref. [8], there is an infinite periodicity in complex K under the shift $K \rightarrow K + ni\pi$, where n is an integer, and, for lattices with even coordination number q , also the shift $K \rightarrow (2n+1)i\pi/2$, as a consequence of the fact that the spin-spin interaction $\sigma_i \sigma_j$ in \mathcal{H} is an integer. In particular, there is an infinite repetition of phases as functions of complex K ; these repeated phases are reduced to a single set by using the variables v , z , or u (or variables based on these).

¹Note that these differ from the respective elliptic moduli κ_0 and $k_{<,0}$ which occur in the internal energy, specific heat, and spontaneous magnetisation for the Ising model on the square lattice at $h = 0$.

We also note an elementary symmetry involving h for the (spin 1/2) Ising model on a general lattice Λ . The low-temperature, high-field expansion of Z has the form

$$Z = e^{(q/2)N_s K} e^{N_s h} Z_r \quad (2.8)$$

where

$$Z_r = 1 + \sum_{n,m} a_{n,m}^{(\Lambda)} z^n \mu^m \quad (2.9)$$

where the only property of Z_r that we need is the fact that it is a polynomial in z and μ . In (2.8), we assume periodic boundary conditions, but for the free energy, in the thermodynamic limit, this is not essential. Also, parenthetically, we note that for a lattice with even q , only even powers of z occur in Z_r , i.e. Z_r is a series in u , but we shall not need this fact here. Now

$$h \rightarrow h + ni\pi \quad \Rightarrow \quad \mu \rightarrow \mu \quad (2.10)$$

where n is an integer. Hence, under such a shift, the only change in Z is in the prefactor, $e^{N_s h}$. Equivalently, in the corresponding (reduced) free energy

$$f = (q/2)K + h + \lim_{N_s \rightarrow \infty} N_s^{-1} (1 + \sum_{n,m} a_{nm}^{(\Lambda)} z^n \mu^m) \quad (2.11)$$

the only change is in the second term, h . Therefore, aside from this term, one may, and we shall, restrict to the range

$$-\frac{i\pi}{2} < \text{Im}(h) \leq \frac{i\pi}{2} \quad (2.12)$$

without loss of generality. In the present context, we shall consider just the value $h = i\pi/2$; our results will apply in the same way to $h = -i\pi/2$.

It is useful to review the connection between the square-lattice Ising model with $h = i\pi/2$ and the Ising model on the square lattice in zero field [6, 7]. This is done by first considering the Ising model on the checkerboard (also called generalised square) lattice, defined by assigning different couplings K_j , $j = 1, \dots, 4$, to the bonds of the square lattice, as shown in Fig. 1. Again, for discussions of the partition function, we assume periodic boundary conditions. The free energy [9] and spontaneous magnetisation [10, 11] are known for the zero-field checkerboard Ising model. Now recall the identity

$$e^{h\sigma} = \cosh h + \sigma \sinh h \quad (2.13)$$

for $\sigma = \pm 1$. For $h = i\pi/2$, this reduces to $e^{h\sigma_n} = i\sigma_n$, and hence $\exp(h \sum_n \sigma_n) = \prod_n (i\sigma_n)$. Next, consider a dimer site covering of the checkerboard lattice, where by site covering, we mean that each site is the member of one (and only one) dimer. As is clear from Fig. 1, a

simple covering of this sort is provided by each of the bonds of a single type, say those with the K_4 couplings. We may thus associate pairs of the σ_n 's in the above product with the dimers of this covering. To do this, we separate one of the two factors of i for such pair and place it in front of Z . One then has

$$Z_{ch} = i^{N_s/2} \sum_{\{\sigma_n\}} \left(\prod_{\langle rs \rangle} (i\sigma_r \sigma_s) \right) \exp\left(\sum_{\langle n, n' \rangle} \sigma_n K_{nn'} \sigma_{n'} \right) \quad (2.14)$$

where ch denotes checkerboard and $K_{nn'}$ refers to the appropriate K_j , $j = 1, 2, 3, 4$ depending on which bond connects the sites n and n' (c.f. Fig. 1). Then one can use the identity (2.13) again to write

$$Z = i^{N_s/2} \sum_{\{\sigma_n\}} \exp\left(\sum_{\langle nn' \rangle} \sigma_n K'_{n,n'} \sigma_{n'} \right) \quad (2.15)$$

that is,

$$Z(\{K_i\}; h = i\pi/2)_{ch} = (i)^{N_s/2} Z(\{K'_i\}; h = 0)_{ch} \quad (2.16)$$

where $K'_i = K_i$, $i = 1, 2, 3$, and

$$K'_4 = K_4 + \frac{i\pi}{2} \quad (2.17)$$

Hence, for the free energy,

$$f(\{K_i\}; h = i\pi/2)_{ch} = \frac{i\pi}{4} + f(\{K'_i\}; h = 0)_{ch} \quad (2.18)$$

Then, setting $K_i = K$, $i = 1, 2, 3, 4$, one can obtain the Lee-Yang result for $f(K, h = i\pi/2)$ [1] from the (analytic continuation of the) free energy for the zero-field checkerboard lattice [9]. The same method works for the magnetisation and yields the relation

$$M(\{K_i\}, h = i\pi/2)_{ch} = M(\{K'_i\}, h = 0)_{ch} \quad (2.19)$$

and for the m -point correlation functions, which satisfy

$$\langle \sigma_{n_1} \cdots \sigma_{n_m} \rangle (\{K_i\}, h = i\pi/2)_{ch} = \langle \sigma_{n_1} \cdots \sigma_{n_m} \rangle (\{K'_i\}, h = 0)_{ch} \quad (2.20)$$

Further, it follows from the special case of (2.20) for 2-spin correlation functions, together with the expression for the susceptibility as a sum over the connected (conn.) 2-spin correlation functions,

$$\bar{\chi} = \sum_{\mathbf{r}} \langle \sigma_{\mathbf{0}} \sigma_{\mathbf{r}} \rangle_{conn.} \quad (2.21)$$

(where $\langle \sigma_{\mathbf{0}} \sigma_{\mathbf{r}} \rangle_{conn.} \equiv \langle \sigma_{\mathbf{0}} \sigma_{\mathbf{r}} \rangle - M^2$) that

$$\bar{\chi}(\{K_i\}, h = i\pi/2)_{ch} = \bar{\chi}(\{K'_i\}, h = 0)_{ch} \quad (2.22)$$

Of course, the Ising model with zero field is not equivalent to one with nonzero field, since in the former case the partition function and free energy are exactly invariant under the Z_2 transformation $\sigma_n \rightarrow -\sigma_n$, whereas in the latter case this symmetry is broken explicitly by the external field term. This inequivalence is manifested in the fact that eqs. (2.16)-(2.17) are not Z_2 -invariant. Thus under the transformation $\sigma_n \rightarrow -\sigma_n$, which is equivalent to $h \rightarrow -h$, the i 's in these equations are replaced by $-i$. It is also manifested in the fact that while the zero-field Ising model always has a Z_2 -symmetric paramagnetic (PM) phase, the model with nonzero external field $h \neq 0$ does not have any PM phase. The usefulness of eq. (2.18) stems from the special feature that for $h = \pm i\pi/2$, this non-invariance is localised to just a constant term in the free energy.

The (reduced) free energy is [1]²

$$f(K, h = \pm i\pi/2) = \pm \frac{i\pi}{2} + \ln 2 + \frac{1}{4} \int_{-\pi}^{\pi} \int_{-\pi}^{\pi} \frac{d\theta_1 d\theta_2}{(2\pi)^2} \ln \left\{ \frac{1}{2} \left[C^4 + S^4 - 1 + S^2 (\cos(\theta_1 + \theta_2) - \cos(\theta_1 - \theta_2)) \right] \right\} \quad (2.23)$$

where C and S were defined in (2.4) and (2.5). From $U = -\partial f / \partial \beta = -J \partial f / \partial K$, one has the symmetries

$$U(\beta, J, H = \frac{i\pi}{2\beta}) = U(\beta, J, H = -\frac{i\pi}{2\beta}) \quad (2.24)$$

$$U(\beta, -J, h = \frac{i\pi}{2}) = U(\beta, J, h = \frac{i\pi}{2}) \quad (2.25)$$

$$U(-\beta, J, h = \frac{i\pi}{2}) = -U(\beta, J, h = \frac{i\pi}{2}) \quad (2.26)$$

Similarly, from $C = k_B K^2 \partial^2 f / \partial K^2$, one has

$$C(K, h = \frac{i\pi}{2}) = C(K, h = -\frac{i\pi}{2}) \quad (2.27)$$

and

$$C(K, h = \frac{i\pi}{2}) = C(-K, h = \frac{i\pi}{2}) \quad (2.28)$$

The free energy is trivially divergent at $K = \pm\infty$, i.e. $u = 0, \infty$; however, this will not be important here since these are isolated points and not part of any phase boundaries. The curves along which the free energy is non-analytic are given by the locus of points where the argument of the logarithm in the integrand of eq. (2.23) vanishes. Expressed in terms of the variable u , f is

$$f(K, h = \pm i\pi/2) = \pm \frac{i\pi}{2} + \frac{1}{4} \ln \left[\frac{(1-u)^2}{u^2} \right] + \frac{1}{4} \int_{-\pi}^{\pi} \int_{-\pi}^{\pi} \frac{d\theta_1 d\theta_2}{(2\pi)^2} \ln \left[(1+u)^2 - 2uP(\theta_1, \theta_2) \right] \quad (2.29)$$

²The Hamiltonian in Ref. [1] was defined with a different zero point of the energy than that used here.

where

$$P(\theta_1, \theta_2) = \cos \theta_1 + \cos \theta_2 \quad (2.30)$$

The above locus of points where the argument of the logarithm vanishes is given by the solutions of the equation

$$(1 + u)^2 - 2ux = 0 \quad (2.31)$$

where $x = P(\theta_1, \theta_2)$, taking values in the range $-2 \leq x \leq 2$. These are integrable singularities. Since the coefficients in this equation are real, the solutions are either real or consist of complex conjugate pairs. Moreover, under the replacement $u \rightarrow 1/u$, eq. (2.31) retains its form, up to an overall factor of u^{-2} . Consequently, the locus of solutions is also invariant under this mapping $u \rightarrow 1/u$. The solutions are shown in Fig. 2(a) and consist of the union of the unit circle

$$u = e^{i\phi}, \quad -\pi < \phi \leq \pi \quad (2.32)$$

and the finite line segment

$$\frac{1}{u_e} \leq u \leq u_e \quad (2.33)$$

where the inner endpoint is

$$u_e = -(3 - 2\sqrt{2}) = -0.171572875... \quad (2.34)$$

and the outer endpoint is $1/u_e = -(3 + 2\sqrt{2}) = -5.828427...$. Note that $u_e = -u_c$, where u_c is the usual critical point in the zero-field square lattice Ising model separating the Z_2 -symmetric, paramagnetic (PM) phase from the phase in which the Z_2 symmetry is spontaneously broken by long-range ferromagnetic (FM) long-range order.

It is of interest to see how the solutions to eq. (2.31) are traced out in the complex u plane as x varies. For $x = 2$, this equation has a double root at $u = 1$. As x decreases from 2 to 0, this root splits into a complex conjugate pair, the members of which move counterclockwise and clockwise along the unit circle, and finally rejoin to form a double root at $u = -1$ when $x = 0$. As x decreases from 0 to -2 , this double root again splits, but this time into two reciprocal real roots, one of which moves to the right, from $u = -1$ to the endpoint u_e and the other of which moves leftward to $u = 1/u_e$. The corresponding phase boundaries in the z plane consist of the unit circle $|z| = 1$ together with the two line segments from $z = \pm z_e = \pm i(\sqrt{2} - 1)$ upward and downward along the imaginary axis to $z = \mp 1/z_e = \pm i(\sqrt{2} + 1)$, respectively.

The circle (2.32) divides the u plane into two separate phases. A fundamental property of this model is that the nonzero external field breaks the Z_2 symmetry explicitly, so that there is no Z_2 -symmetric phase. Even without using the known expression for the magnetisation,

one can identify the phases in this diagram as follows. For sufficiently large real K , the interaction of the external magnetic field with the spins is negligible compared with the spin-spin interaction, which thus produces a ferromagnetically ordered phase, just as it does in the model with $h = 0$. This shows that the neighborhood of the origin in the u (or z) plane is ferromagnetically ordered. By analytic continuation, it then follows that the entire region inside the unit circle $|u| = 1$ is a ferromagnetically ordered phase, and this is so denoted in Fig. 2(a). Similarly, for sufficiently large negative K , the interaction of the external field with the spins is again negligible compared with the spin-spin interaction, which produces a phase with antiferromagnetic (AFM) long-range order. By analogous analytic continuation arguments, it follows that the entire region outside the unit circle is the AFM phase. This may be shown as follows. One may think of the phase diagram in the complex variable $w = 1/u$. By the $u \rightarrow 1/u$ symmetry noted above, the phase boundaries in this variable are the same as those in Fig. 2(a). The above argument shows that the neighborhood of the origin is antiferromagnetically ordered, and hence, by the same analytic continuation method, the entire region inside the unit circle $|w| = 1$ is an AFM phase. Mapping this back to the u plane, one has shown that the entire region outside of the unit circle $|u| = 1$ is the AFM phase. Since the u plane consists of precisely two regions with the property that within each one can analytically continue from any one point to any other, we have thus obtained a complete description of the phases in the model. The same reasoning implies that in the z plane, the phase with $|z| < 1$ is FM and the phase with $|z| > 1$ is AFM. In passing, we note that complex-temperature properties of the $h = 0$ Ising model on $d = 2$ lattices have been studied in Refs. [12, 13, 14, 15, 16, 8, 17, 18, 19, 20]. In the case $h = 0$ for the square lattice, the analogous locus of points across which the free energy is singular form a limaçon [18] defined by $Re(u) = 1 + 2^{3/2} \cos \omega + 2 \cos 2\omega$, $Im(u) = 2^{3/2} \sin \omega + 2 \sin 2\omega$ for $0 \leq \omega < 2\pi$, or equivalently, in the z plane, the circles [12] $z = \pm 1 + \sqrt{2}e^{i\theta}$, for $0 \leq \theta < 2\pi$.

By the use of the conformal mapping (2.2) on the z plane, or by re-expressing the free energy in terms of the variable v and again solving for the locus of points where the argument of the logarithm vanishes, we find that the phase diagram of the model in the v plane is as shown in Fig. 2(b). The unit circle $|z| = 1$ is mapped to the imaginary axis in the v plane, and the respective line segments from $z = \pm z_e$ to $\mp 1/z_e$ are mapped to the arcs from $v = e^{\mp i\pi/4}$ to $v = e^{\mp 3i\pi/4}$. It is interesting that the $Re(v) = 0$ (i.e. imaginary) axis forms the boundary between the complex-temperature FM and AFM phases. One may understand this by recalling that (i) if h were real and positive (negative), this would favor FM (AFM) ordering, but a pure imaginary value of h does not favor FM over AFM ordering, or vice versa; (ii) similarly, if the spin-spin coupling K is real and positive (negative), it favors FM (AFM) ordering, but a pure imaginary value of K (and hence v) does not favor FM over

AFM ordering, or vice versa. Therefore, if both h and K are pure imaginary, as is the case here for the imaginary axis in the v plane, then the system is precisely balanced between FM and AFM order, so that this axis should be the boundary between the complex-temperature FM and AFM phases, and this is just what our explicit calculation shows.

The mapping defined by $u \rightarrow \kappa^2$, where κ was defined in (2.3), takes the the locus of points (2.32) and (2.33) to a single semi-infinite line segment extending from 1 to ∞ in the complex κ^2 plane. All points in the κ^2 plane are analytically connected to all other points. In particular, the mapping $u \rightarrow \kappa^2$ takes both the complex-temperature FM and AFM phases in the u plane to the same respective regions in the κ^2 plane, as is clear from the symmetry (2.6) and the fact that the transformation $u \rightarrow 1/u$ interchanges the FM and AFM phases in the u plane.

3 Complex-Temperature Behaviour of the Internal Energy and Specific Heat

3.1 Exact Expressions

From the free energy (2.29), it is straightforward to calculate the internal energy U and specific heat C (per site). In terms of the variable u , we find that

$$U = -J \left[\frac{1+u}{1-u} + \left(\frac{1-u}{1+u} \right) \left(\frac{2}{\pi} \right) K(\kappa) \right] \quad (3.1.1)$$

where the elliptic modulus κ was given above in eq. (2.3) and $K(k) = \int_0^{\pi/2} (1-k^2 \sin^2 \theta)^{-1/2} d\theta$ is the complete elliptic integral of the first kind. This expression holds for both the FM and AFM phases and exhibits the symmetries (2.25) and (2.26). Since either of these has the effect of taking $u \rightarrow 1/u$, and since this mapping takes the interior of the complex-temperature FM phase to the interior of the complex-temperature AFM phase, the values of U in these two phases are simply related by (2.25)-(2.26). In the FM phase, the first few terms of the small- $|u|$ expansion (complex-temperature generalisation of the low-temperature expansion) are

$$U = -2J \left[1 + 4u^2 - 12u^3 + 60u^4 - 280u^5 + O(u^6) \right] \quad (3.1.2)$$

In the AFM phase, the corresponding expansion parameter is $w = 1/u$, and U has the same expansion as (3.1.2) with J replaced by $-J$ and u replaced by w .

As discussed above, in the limit $J \rightarrow \infty$, and hence $K \rightarrow \infty$ with fixed H , the spin-spin interaction overwhelms the contribution of the external field coupling, which therefore has a negligible effect, to leading order. It follows that in this limit, the value of the internal

energy should be the same as the value for $h = 0$, i.e.,

$$U(u = 0, h = i\pi/2) = U(u = 0, h = 0) \quad (3.1.3)$$

It is interesting to compare the small- $|u|$ series expansions of these two functions to ascertain the finite- u corrections to this equality. For this purpose, we recall that [2]

$$U(K, h = 0) = -J \left[\frac{1+u}{1-u} + \frac{(1-6u+u^2)}{(1-u^2)} \left(\frac{2}{\pi} \right) K(\kappa_0) \right] \quad (3.1.4)$$

where

$$\kappa_0 = \frac{4z(1-u)}{(1+u)^2} \quad (3.1.5)$$

The expression (3.1.10) holds for all phases, PM, FM, and AFM. In the FM phase, it has the small- $|u|$ expansion

$$U(h = 0) = -2J \left[1 - 4u^2 - 12u^3 - 36u^4 - 120u^5 + O(u^6) \right] \quad (3.1.6)$$

Clearly, the expansions (3.1.2) and (3.1.6) agree with the relation (3.1.3) for $u = 0$. $U(K, h = 0)$ also satisfies the symmetries analogous to (2.25) and (2.26), with $h = i\pi/2$ replaced by $h = 0$; as a consequence, in the AFM phase, the small- $|w|$ expansion of $U(K, h = 0)$ is given by (3.1.6) with J replaced by $-J$ and u replaced by w .

For C we get

$$\frac{C}{8k_B K^2} = -\frac{u}{(1-u)^2} - \frac{(1+u)^2}{\pi(1+6u+u^2)} E(\kappa) + \frac{(1+u^2)}{\pi(1+u)^2} K(\kappa) \quad (3.1.7)$$

where $K(k)$ was defined above and $E(k) = \int_0^{\pi/2} (1 - k^2 \sin^2 \theta)^{1/2} d\theta$ is the complete elliptic integral of the second kind. Again, this expression holds for both the FM and AFM phases. It will also be useful to express C in an equivalent form, using (2.3):

$$\frac{C}{8k_B K^2} = -\frac{u}{(1-u)^2} - \frac{E(\kappa)}{\pi(1+\kappa)} + \frac{(1+u^2)(1+\kappa)K(\kappa)}{\pi(1+6u+u^2)} \quad (3.1.8)$$

C/K^2 has the small- $|u|$ expansion

$$\frac{C}{8k_B K^2} = -64u^2 + 288u^3 - 1920u^4 + 11200u^5 + O(u^6) \quad (3.1.9)$$

For comparison, the specific heat for the Ising model on the square lattice with $h = 0$ [2] is

$$\frac{C}{k_B K^2} = \frac{4(1-\kappa')}{\pi\kappa^2} \left[2\{K(\kappa_0) - E(\kappa_0)\} - (1-\kappa'_0)\left\{\frac{\pi}{2} + \kappa'_0 K(\kappa_0)\right\} \right] \quad (3.1.10)$$

which has the small- $|u|$ expansion

$$\frac{C}{k_B K^2} = 64u^2 + 288u^3 + 1152u^4 + 4800u^5 + O(u^6) \quad (3.1.11)$$

Of course, in this case, the positivity of the specific heat requires that the coefficient of the lowest order term must be positive (the first negative coefficient occurs in the u^7 term). We proceed to determine the complex-temperature singularities of U and C for the present case, $h = i\pi/2$.

3.2 Vicinity of $u = u_e$

As discussed in connection with Fig. 2(a), the point $u = u_e$ is the endpoint of the singular line segment protruding into the complex-temperature extension of the FM phase. All approaches to this point, except directly from the left along this singular line segment, occur from within the complex-temperature FM phase. As $u \rightarrow u_e = -(3 - 2^{3/2})$, $\kappa \rightarrow -1$. The internal energy diverges like

$$\frac{U}{J} \rightarrow \frac{\sqrt{2}}{\pi} \ln(1 - u/u_e), \quad \text{as } u \rightarrow u_e \quad (3.2.1)$$

In the specific heat, the dominant divergence arises from the term in (3.1.7) involving $E(\kappa)$ and is

$$\frac{C}{k_B K^2} \rightarrow -\frac{4\sqrt{2}}{\pi(1 - u/u_e)}, \quad \text{as } u \rightarrow u_e \quad (3.2.2)$$

so that the associated singular exponent for C at $u = u_e$ is

$$\alpha'_{e,FM} \equiv \alpha'_e = 1 \quad (3.2.3)$$

where the subscript FM indicates the phase from which this point is approached, and the prime is the standard notation indicating that the approach to this singular point is from within a broken-symmetry phase. (The last feature is, of course, true of all of the singular points for $h \neq 0$.) There is also a weaker, logarithmic divergence arising from the term involving $K(\kappa)$. The value of K at u_e in (3.2.2) is

$$K_e = -\frac{1}{4} \ln u_e = -\frac{1}{4} \left[\ln(3 - 2^{3/2}) + i\pi + 2ni\pi \right] \quad (3.2.4)$$

where n labels the Riemann sheet used for the evaluation of the logarithm, which we shall take to be $n = 0$ below, unless otherwise indicated.

3.3 Vicinity of $u = 1/u_e$

The point $u = 1/u_e$ is the left end of the singular line segment protruding into the complex-temperature extension of the AFM phase. Except for the approach directly from the right along the singular line segment, all approaches to this point occur from within the complex-temperature AFM phase. As $u \rightarrow 1/u_e$, $\kappa \rightarrow -1$, as is clear from the previous remarks and the symmetry (2.6). The internal energy again diverges like

$$\frac{U}{J} \rightarrow -\frac{\sqrt{2}}{\pi} \ln(1 - u_e u), \quad \text{as } u \rightarrow \frac{1}{u_e} \quad (3.3.1)$$

In the specific heat, the dominant divergence again arises from the term in (3.1.7) involving $E(\kappa)$ and is

$$\frac{C}{k_B K^2} \rightarrow \frac{4\sqrt{2}}{\pi(1 - u_e u)}, \quad \text{as } u \rightarrow 1/u_e \quad (3.3.2)$$

so that the associated singular exponent for C at the outer endpoint (oe) $u = 1/u_e$ is

$$\alpha'_{oe,AFM} \equiv \alpha'_{oe} = 1 \quad (3.3.3)$$

The value of K corresponding to $u = 1/u_e$ in eq. (3.3.2) is, for the principal Riemann sheet of the log, $K_{oe} = -(1/4)[\ln(3 + 2^{3/2}) + i\pi]$.

3.4 Vicinity of $u = -1$

As $u \rightarrow -1$ (denoted u_s), κ diverges; if we set $u = -1 + \epsilon e^{i\phi}$ and let $\epsilon \rightarrow 0$, then $\kappa \sim -4\epsilon^{-2} e^{-2i\phi}$. One easily sees that $U(u = -1)$ is finite. For C , we observe that the first and second terms on the right-hand side of eq. (3.1.7) or (3.1.8) are finite. By the use of the elliptic integral identity $(1 + \kappa)K(\kappa) = K(2\kappa^{1/2}/(1 + \kappa))$ (see, e.g. [21]), we can rewrite the term involving $K(\kappa)$ in eq. (3.1.8) as

$$\frac{(1 + u^2)}{\pi(1 + 6u + u^2)} K\left(\frac{2\kappa^{1/2}}{1 + \kappa}\right) \quad (3.4.1)$$

As $u \rightarrow -1$ and κ diverges, $K(2\kappa^{1/2}/(1 + \kappa)) \rightarrow K(0) = \pi/2$, so that C is finite, although non-analytic, at $u = -1$. This is true for the approach to $u = -1$ from either the FM or AFM phases. We thus have

$$\alpha'_{s,FM} = \alpha'_{s,AFM} = 0 \quad (\text{log. finite}) \quad (3.4.2)$$

3.5 Vicinity of $u = 1$

As $u \rightarrow 1$, $\kappa \rightarrow 1$. In U the leading potential singularity arises from the first term in (3.1.1)

$$\frac{U}{J} \rightarrow \frac{-2}{1-u} \quad \text{as } u \rightarrow 1 \quad (3.5.1)$$

Now $K = -(1/4) \ln u$, so that, if one uses the first Riemann sheet of the logarithm, then $u \rightarrow 1$ maps to $K \rightarrow 0$. Recalling that $K = \beta J$, if this zero in K is due to $\beta \rightarrow 0$ at fixed nonzero J , then eq. (3.5.1) shows that U diverges for $u \rightarrow 1$; however, if the zero in K is due to $J \rightarrow 0$ at fixed nonzero β , then, expanding (3.5.1), one finds that $U \rightarrow 1/(2\beta)$.

For the specific heat, from (3.1.7), it follows that as $u \rightarrow 1$,

$$k_B^{-1}C \rightarrow 8K^2 \left[-\frac{1}{(1-u)^2} + \frac{1}{4\pi} \ln\left(\frac{32}{(1-u)^2}\right) + \dots \right] \quad (3.5.2)$$

where ... refers to less singular terms. If we again use the principal Riemann sheet of the logarithm, so that $u \rightarrow 1$ corresponds to $K \rightarrow 0$, then (3.5.2) becomes

$$k_B^{-1}C \rightarrow -\frac{1}{2} + \frac{2}{\pi} K^2 \ln\left(\frac{2}{K^2}\right) + O(K^2) \quad \text{as } u \rightarrow 1 \quad (3.5.3)$$

That is, C has a finite logarithmic singularity at this point, and hence a corresponding exponent

$$\alpha'_{1,FM} = \alpha'_{1,AFM} = 0 \quad (\text{log. finite}) \quad (3.5.4)$$

In passing, we note that if one were to use a Riemann sheet different than the principal ($n = 0$) one in evaluating $K = -(1/4) \ln(1)$, so that $K = -in\pi/2 \neq 0$, then C would diverge quadratically at $u = 1$.

3.6 Elsewhere Along the Singular Curves

We discuss here the behaviour of U and C as one crosses the singular locus of points comprised by the unit circle (2.32) and the line segment (2.33) away from the points $u = u_e, 1/u_e, -1$, and 1. The singularities which one encounters in this case are associated with passage across the branch cut of the elliptic integrals in (3.1.1) and (3.1.7). We recall that the elliptic integrals $K(\kappa)$ and $E(\kappa)$ are analytic functions of κ^2 in the complex κ^2 plane except for respectively divergent and finite branch points at $\kappa^2 = 1$ and an associated branch cut, which is normally taken to run from $\kappa^2 = 1$ to $\kappa^2 = \infty$ along the positive real axis in this plane. To illustrate the nature of the singularities, we shall consider moving outward along a ray in the u plane defined by $u = \rho e^{i\theta}$ with ρ increasing from 0 to ∞ at fixed θ , say $\theta = \pi/6$. As shown in Fig. 3, the image point in the κ^2 plane also moves out from the origin, starting

with an angle of $\pi/3$ but bending around to the right. As we cross the unit circle in the u plane, leaving the FM phase and entering the AFM phase, the image point in the κ^2 plane crosses the branch cut moving vertically downward. This branch cut is precisely the image of the unit circle $|u| = 1$ (and also of the singular line segment (2.33).) For $\theta = \pi/6$, the crossing point is at $\kappa^2 = 2^4(7 - 4\sqrt{3}) = 1.1487\dots$. In the κ^2 plane, one thus passes onto the second Riemann sheet of the elliptic functions $K(\kappa)$ and $E(\kappa)$. If one projects back to the first Riemann sheet, these functions have discontinuous imaginary parts across this branch cut. As ρ continues to increase toward ∞ , $\kappa^2 \sim 16\rho^{-2}e^{-2\theta}$ so that the image point curves around finally approaches the origin in a “northwest” direction, at an angle of $-\pi/3$, but on the second Riemann sheet. In Fig. 3 we show the image point for ρ in the range from 0 to 30.

4 Complex-Temperature Behaviour of the Uniform and Staggered Magnetisation

The magnetisation M is [1, 5]

$$M(u, h = i\pi/2) = \frac{(1+u)^{1/2}}{(1-u)^{1/4}(1+6u+u^2)^{1/8}} \quad (4.1)$$

Note that $(1+6u+u^2) = (1-u/u_e)(1-u_e u)$. By analytic continuation, this formula holds throughout the complex-temperature extension of the FM phase. The identity discussed above, and the resultant eq. (2.19) yields the relation

$$M(u, h = \pm i\pi/2) = M(-u, h = 0)^{-1} \quad (4.2)$$

where [3]

$$M(u, h = 0) = \frac{(1+u)^{1/4}(1-6u+u^2)^{1/8}}{(1-u)^{1/2}} \quad (4.3)$$

As is well known, one can express $M(u, h = 0)$ as

$$M(u, h = 0) = (1 - (k_{<,0})^2)^{1/8} \quad (4.4)$$

where

$$k_{<,0} = \frac{1}{\sinh^2(2K)} = \frac{4u}{(1-u)^2} \quad (4.5)$$

This quantity also enters in exact expressions for correlation functions in the FM phase of the $h = 0$ Ising model [22, 23, 24]. Given the relation (4.2), it is natural to write

$$M(u, h = i\pi/2) = (1 - (k_{<})^2)^{1/8} \quad (4.6)$$

where the elliptic modulus was introduced in eq. (2.7). The magnetisation for the $h = i\pi/2$ case vanishes continuously at the point $u = -1$ (denoted u_s) with exponent

$$\beta_s = \frac{1}{2} \quad (4.7)$$

diverges at $u = u_e$ with exponent

$$\beta_e = -\frac{1}{8} \quad (4.8)$$

and diverges at $u = 1$ with exponent

$$\beta_1 = -\frac{1}{4} \quad (4.9)$$

Elsewhere on the boundary of the complex-temperature extension of the FM phase, i.e., the unit circle in the u plane, M vanishes discontinuously. Note that the apparent divergence at the point $u = 1/u_e$ does not actually occur, since this is outside of the complex-temperature FM phase, where the above analytic continuation is valid.

The staggered magnetisation M_{st} does not seem to have been explicitly discussed in the literature, but one can easily obtain it, as follows. M_{st} may be defined via

$$M_{st}^2 = \lim_{|\mathbf{r}| \rightarrow \infty} \langle \tilde{\sigma}_0 \tilde{\sigma}_{\mathbf{r}} \rangle \quad (4.10)$$

where

$$\tilde{\sigma}_{\mathbf{r}} = (-1)^{p(\mathbf{r})} \sigma_{\mathbf{r}} \quad (4.11)$$

where

$$p(\mathbf{r}) = \sum_{i=1}^2 r_i \quad (4.12)$$

i.e. $\tilde{\sigma}_{\mathbf{r}} = \sigma_{\mathbf{r}}$ for \mathbf{r} on the same sublattice as $\mathbf{r} = \mathbf{0}$ and $-\sigma_{\mathbf{r}}$ for \mathbf{r} on the other sublattice of the (bipartite) square lattice. To evaluate M_{st} via eq. (4.10), it suffices to take $\mathbf{r} = (r, 0)$ or $(0, r)$, i.e. the row or column 2-spin correlation function. From the known asymptotic behaviour of this correlation function [5], one immediately finds that

$$M_{st}(w) = M(u \rightarrow w) \quad (4.13)$$

where, as before, $w = 1/u$. This is consistent with eq. (4.6) since (c.f. (2.6)) $u \rightarrow 1/u$ takes $k_{<} \rightarrow -k_{<}$, and $k_{<}$ enters squared in (4.6). Of course, M_{st} vanishes identically outside the complex-temperature extension of the AFM phase. Further, we may immediately conclude that M_{st} vanishes continuously at $u = -1$ with exponent (4.7), diverges at $u = 1/u_e$ with exponent (4.8), and diverges at $u = 1$ with exponent (4.9). Elsewhere along the boundary of the complex-temperature AFM phase, M_{st} vanishes discontinuously, with the same discontinuity as M .

It is of interest to compare these results with the behaviour of M and M_{st} for $h = 0$ (again on the square lattice). Aside from the physical PM-FM and PM-AFM critical points $u = u_c = (3 - 2^{3/2})$ and $1/u_c$, where, respectively, M and M_{st} vanish continuously with exponent $\beta = 1/8$, they also both vanish continuously at the complex-temperature point $u = -1$, with the same exponent, $\beta = 1/4$. Note that for $h = 0$ there is only one point, viz., $u = -1$, where the FM and AFM phases are contiguous and M and M_{st} vanish continuously, whereas for $h = i\pi/2$ there are two such points, namely, $u = -1$ and $u = 1$.

5 Extraction and Analysis of the Low-Temperature Series for $\bar{\chi}$

5.1 Generalities

In order to investigate the complex-temperature singularities of the susceptibility $\bar{\chi}$, we shall make use of the low-temperature, high-field series expansion for the free energy or equivalently the partition function of the Ising model on the square lattice [25, 26, 27]. In Ref. [27], Baxter and Enting calculated this expansion for the partition function to order $O(u^{23})$. The series for Z_r in eq. (2.9) is

$$Z_r = 1 + \sum_{n=2}^{\infty} \sum_m a_{n,m} u^n \mu^m \quad (5.1.1)$$

where $j \leq m \leq j^2$ for $n = 2j$ and $j \leq m \leq j(j-1)$ for $n = 2j-1$. We extract the series for $h = i\pi/2$ by calculating $\bar{\chi} = \partial^2 f / \partial h^2$ and then substituting $\mu = -1$. This has the form

$$\bar{\chi}(u, h = i\pi/2) = 4u^2 \left(\sum_{n=0}^{\infty} c_n u^n \right) \quad (5.1.2)$$

The results for the c_n are listed in Table 1; the series for Z and the resultant series for $\bar{\chi}$ to $O(u^{23})$ yields the c_n 's to order $n = 21$. Parenthetically, we note that $\bar{\chi}$ has been calculated to $O(u^{28})$ in Ref. [28] and to $O(u^{38})$ in Ref. [17], but the low-temperature, high-field expansion of the partition function as a function of $\mu = e^{-2h}$ which would be necessary to extract $\bar{\chi}(h = i\pi/2)$ was not given in these papers (it would be a rather long expression).

We have analysed this series using dlog Padé and differential approximants. For a recent review of these techniques, see Ref. [29]. Our notation for these approximants follows Ref. [29] and our earlier work on complex-temperature properties of the $h = 0$ Ising model [18, 19, 20]. In particular, we use first order differential approximants (i.e., $K = 1$ in our previous notation); as before, we used unbiased approximants so as to be able to use an

n	c_n
0	-1
1	8
2	-48
3	304
4	-1863
5	11368
6	-68840
7	414872
8	-2490437
9	14903648
10	-88963696
11	529939176
12	-3151205475
13	18710180192
14	-110948037424
15	657164715520
16	-3888670886593
17	22990566432904
18	-135819110416784
19	801806651588848
20	-4730485389238263
21	27892958533539784

Table 1: Low-temperature series expansion coefficients for $\bar{\chi}(u, h = i\pi/2)$ in eq. (5.1.2).

extrapolation method for extracting critical exponents. Since the prefactor $4u^2$ is analytic, we have actually performed the analysis on the reduced function

$$\bar{\chi}_r \equiv \frac{\bar{\chi}}{4u^2} = \sum_{n=0}^{\infty} c_n u^n \quad (5.1.3)$$

As one approaches a generic complex singular point denoted *sing* from within the complex-temperature extension of the FM phase, $\bar{\chi}$ is assumed to have the leading singularity

$$\bar{\chi} \sim A'_{sing} (1 - u/u_{sing})^{-\gamma'_{sing}} \left(1 + a_1 (1 - u/u_{sing}) + \dots \right) \quad (5.1.4)$$

where A'_{sing} and γ'_{sing} denote, respectively, the critical amplitude and the corresponding critical exponent, and the ... represent analytic confluent corrections. One may observe that we have not included non-analytic confluent corrections to the scaling form in eq. (5.1.4). The reason is that, as discussed in our earlier work [18], previous studies have indicated that they are very weak or absent for the 2D Ising model. We proceed to our results.

5.2 Singularity at $u = u_e$

Our dlog Padé results relevant to the singularity in $\bar{\chi}(u, h = i\pi/2)$ at $u = u_e$ are given in Table 2. Because of the length of our differential approximant results relevant to the singularity in $\bar{\chi}$ at $u = u_e$, we list these in the Appendix. From these results, we infer the location of the singularity to be

$$u_{sing.} = -0.17157 \pm 0.00001 \quad (5.2.1)$$

This, together with our knowledge of the exact location of the endpoint of the singular line segment (2.33), supports the conclusion that the exact location of this singularity is at $u = u_e = -0.1715729\dots$ given in (2.34). Accepting this conclusion, we plot the values of the corresponding exponent γ'_e for the differential approximants as functions of the normalised distance from this point, i.e., $|u_{sing.} - u_e|/|u_e|$ and extrapolate to zero distance. (This extrapolation method is similar to the use of biased differential approximants; in both of these approaches, one uses one's knowledge of the exact position of the singularity.) From our extrapolation, we obtain

$$\gamma'_e = 1.25 \pm 0.01 \quad (5.2.2)$$

This strongly supports the following inference for the exact value of this exponent, which we shall make:

$$\gamma'_e = \frac{5}{4} \quad (5.2.3)$$

$[N/D]$	u_{sing}	$ u_{sing} - u_e / u_e $	γ'_e
[5/3]	-0.1716072	2.0×10^{-4}	1.2492
[4/4]	-0.1715705	1.4×10^{-5}	1.2464
[5/4]	-0.1715636	5.4×10^{-5}	1.2459
[6/4]	-0.1715646	4.8×10^{-5}	1.2460
[3/5]	-0.1715802	4.3×10^{-5}	1.2471
[4/5]	-0.1715628	5.8×10^{-5}	1.2458
[5/5]	-0.1715645	4.9×10^{-5}	1.2460
[6/5]	-0.1715598	7.6×10^{-5}	1.2457
[7/5]	-0.1715670	3.4×10^{-5}	1.2462
[4/6]	-0.1715647	4.8×10^{-5}	1.2460
[5/6]	-0.1715674	3.2×10^{-5}	1.2462
[6/6]	-0.1715667	3.6×10^{-5}	1.2462
[7/6]	-0.1715667	3.6×10^{-5}	1.2462
[8/6]	-0.1715665	3.7×10^{-5}	1.2462
[5/7]	-0.1715668	3.6×10^{-5}	1.2462
[6/7]	-0.1715667	3.6×10^{-5}	1.2462
[7/7]	-0.1715670	3.4×10^{-5}	1.2462
[8/7]	-0.1715664	3.8×10^{-5}	1.2461
[9/7]	-0.1715664	3.7×10^{-5}	1.2461
[6/8]	-0.1715672	3.3×10^{-5}	1.2462
[7/8]	-0.1715664	3.8×10^{-5}	1.2461
[8/8]	-0.1715665	3.7×10^{-5}	1.2461
[9/8]	-0.1715754	1.5×10^{-5}	1.2501
[10/8]	-0.1715673	3.2×10^{-5}	1.2463
[7/9]	-0.1715665	3.7×10^{-5}	1.2461
[8/9]	-0.1715666	3.6×10^{-5}	1.2462
[9/9]	-0.1715673	3.2×10^{-5}	1.2463
[10/9]	-0.1715677	3.0×10^{-5}	1.2464
[11/9]	-0.1715696	1.9×10^{-5}	1.2470
[8/10]	-0.1715674	3.2×10^{-5}	1.2463
[9/10]	-0.1715686	2.5×10^{-5}	1.2466
[10/10]	-0.1715699	1.7×10^{-5}	1.2471
[9/11]	-0.1715701	1.6×10^{-5}	1.2472

Table 2: Values of pole near $u_e = -(3 - 2^{3/2}) = -0.171572875\dots$, normalised distance from this point, $|u_{sing} - u_e|/|u_e|$, and exponent γ'_e from dlog Padé approximants to low-temperature series for $\bar{\chi}_r(u, h = i\pi/2)$, starting with the series to $O(u^9)$. We list only the approximants which satisfy the accuracy criterion $|u_{sing} - u_e|/|u_e| \leq 2 \times 10^{-4}$.

$[N/D]$	u_{sing}	$ u_{sing} - 1 $	γ'_1
[4/5]	1.0024444	2.4×10^{-3}	2.3646
[6/6]	0.9894269	1.1×10^{-2}	2.3347
[5/7]	0.9920029	8.0×10^{-3}	2.3623
[6/7]	0.9817550	1.8×10^{-2}	2.2642
[7/7]	0.9878026	1.2×10^{-2}	2.3213
[8/7]	0.9988081	1.2×10^{-3}	2.4483
[6/8]	0.9892965	1.1×10^{-2}	2.3380
[8/8]	0.9922151	7.8×10^{-3}	2.3641
[9/8]	0.9969711	3.0×10^{-3}	2.4255
[10/8]	0.9974836	2.5×10^{-3}	2.4332
[7/9]	0.9934910	6.5×10^{-3}	2.3814
[8/9]	1.0054945	5.5×10^{-3}	2.5876
[9/9]	0.9975390	2.5×10^{-3}	2.4342
[10/9]	0.9967646	3.2×10^{-3}	2.4231
[11/9]	0.9982017	1.8×10^{-3}	2.4446
[8/10]	0.9980098	2.0×10^{-3}	2.4427
[9/10]	0.9992196	7.8×10^{-4}	2.4648
[10/10]	0.9984417	1.6×10^{-3}	2.4495
[9/11]	0.9985604	1.4×10^{-3}	2.4519

Table 3: Values of pole near $u = 1$, normalised distance from this point, $|u_{sing} - 1|$, and exponent γ'_1 from $[M/N]$ dlog Padé approximants to low-temperature series for $\bar{\chi}_r$. We list only the differential approximants which satisfy the accuracy criterion $|u_{sing} - 1| < 2 \times 10^{-2}$.

To calculate the critical amplitude for $\bar{\chi}$ at the $u = u_e$ singularity, we use the standard method of analysing Padé approximants to the series $(-\bar{\chi}_r)^{1/\gamma'_e}$ (where the minus sign is inserted because $c_0 = -1$ in eq. (5.1.2)). For A'_e as defined in eq. (5.1.4) with $u_{sing} = u_e$, we obtain

$$A'_e = -0.11515 \pm 0.00020 \quad (5.2.4)$$

5.3 Singularity at $u = 1$

Our dlog Padé results for $\bar{\chi}_r$ relevant to the singularity at $u = 1$ are given in Table 3. We obtain more precise results from differential approximants; these are given in Table 4 and its continuation. From these results, we obtain the location of the singularity as

$[L/M_0; M_1]$	u_{sing}	$ u_{sing} - 1 $	γ'_1
[0/7; 7]	1.0019932	2.0×10^{-3}	2.5262
[0/7; 9]	0.9983638	1.6×10^{-3}	2.4478
[0/8; 9]	0.9974253	2.6×10^{-3}	2.4337
[0/8; 10]	0.9981341	1.9×10^{-3}	2.4447
[0/9; 9]	0.9999105	0.89×10^{-4}	2.4776
[0/9; 10]	0.9984608	1.5×10^{-3}	2.4502
[0/10; 9]	0.9982548	1.7×10^{-3}	2.4461
[1/4; 5]	1.0013165	1.3×10^{-3}	2.4393
[1/6; 8]	0.9989524	1.0×10^{-3}	2.4554
[1/7; 9]	0.9981225	1.9×10^{-3}	2.4445
[1/8; 8]	1.0019138	1.9×10^{-3}	2.5153
[1/8; 9]	0.9982128	1.8×10^{-3}	2.4460
[1/8; 10]	0.9981111	1.9×10^{-3}	2.4444
[1/9; 9]	0.9990590	0.94×10^{-3}	2.4617
[2/4; 6]	1.0004562	0.46×10^{-3}	2.4545
[2/6; 4]	1.0008071	0.81×10^{-3}	2.4534
[2/6; 6]	1.0012170	1.2×10^{-3}	2.4958
[2/6; 7]	0.9997299	2.7×10^{-4}	2.4678
[2/6; 8]	0.9973495	2.7×10^{-3}	2.4543
[2/7; 6]	0.9996006	4.0×10^{-4}	2.4651
[2/7; 9]	0.9981442	1.9×10^{-3}	2.4450
[2/8; 8]	1.0006495	0.65×10^{-3}	2.4969
[2/8; 9]	0.9985512	1.4×10^{-3}	2.4513
[2/9; 8]	0.9983746	1.6×10^{-3}	2.4474
[3/6; 6]	1.0005153	0.52×10^{-3}	2.4841
[3/6; 7]	0.9973962	2.6×10^{-3}	2.4232
[3/6; 8]	0.9974009	2.6×10^{-3}	2.4201
[3/7; 6]	0.9971786	2.8×10^{-3}	2.4189
[3/7; 7]	0.9977559	2.2×10^{-3}	2.4302
[3/7; 8]	0.9981732	1.8×10^{-3}	2.4407
[3/7; 9]	0.9980242	2.0×10^{-3}	2.4651
[3/8; 6]	0.9975202	2.5×10^{-3}	2.4227

Table 4: Values of pole near $u = 1$, normalised distance from this point, $|u_{sing} - 1|$, and exponent γ'_1 from differential approximants to low-temperature series for $\bar{\chi}_r$. We list only the differential approximants which satisfy the accuracy criterion $|u_{sing} - 1| \leq 2 \times 10^{-3}$.

[3/8; 7]	0.9980148	2.0×10^{-3}	2.4375
[3/8; 8]	0.9986544	1.3×10^{-3}	2.4508
[3/9; 7]	0.9991902	0.81×10^{-3}	2.4621
[4/4; 4]	1.0024665	2.5×10^{-3}	2.4681
[4/5; 7]	0.9979715	2.0×10^{-3}	2.4379
[4/6; 8]	0.9998460	1.5×10^{-4}	2.4832
[4/7; 5]	0.9982928	1.7×10^{-3}	2.4505
[4/7; 7]	0.9989074	1.1×10^{-3}	2.4584
[4/7; 8]	0.9990659	0.93×10^{-3}	2.4624
[4/8; 7]	0.9990450	0.96×10^{-3}	2.4618
[5/4; 5]	1.0009762	0.98×10^{-3}	2.4429
[5/5; 7]	0.9987068	1.3×10^{-3}	2.4543
[5/6; 7]	0.9993881	0.61×10^{-3}	2.4709
[5/6; 8]	0.9991317	0.87×10^{-3}	2.4644
[5/7; 6]	1.0014642	1.5×10^{-3}	2.5280
[5/7; 7]	0.9990811	0.92×10^{-3}	2.4629
[5/8; 6]	1.0000180	1.8×10^{-5}	2.4888
[6/4; 6]	0.9993653	0.63×10^{-3}	2.5040
[6/5; 7]	1.0002641	2.6×10^{-4}	2.4944
[6/6; 7]	0.9991189	0.88×10^{-3}	2.4641
[6/7; 5]	1.0003178	3.2×10^{-4}	2.4956
[6/7; 6]	0.9993080	0.69×10^{-3}	2.4698
[7/5; 6]	0.9990014	1.0×10^{-3}	2.4565
[7/6; 5]	0.9983233	1.7×10^{-3}	2.4405
[8/4; 6]	0.9993253	0.67×10^{-3}	2.4757
[8/5; 5]	0.9987939	1.2×10^{-3}	2.4448
[8/5; 6]	0.9994784	0.52×10^{-3}	2.4852
[8/6; 5]	0.9981646	1.8×10^{-3}	2.4390
[9/4; 6]	0.9986630	1.3×10^{-3}	2.4600

Table 5: Continuation of table of differential approximants for the singularity in $\bar{\chi}_r$ at $u = 1$.

$$u_{sing} = 0.999 \pm 0.001 \quad (5.3.1)$$

From this and our determination of the phase boundaries (2.32)-(2.33), we infer that the exact location of this singularity is at $u = 1$. Given this conclusion, we then plot the values of γ'_1 as a function of the distance from $u = 1$ and extrapolate to zero distance. This yields the value

$$\gamma'_1 = 2.50 \pm 0.01 \quad (5.3.2)$$

This strongly supports the following inference that we shall make for the exact value of this exponent:

$$\gamma'_1 = \frac{5}{2} \quad (5.3.3)$$

Hence, in particular,

$$\gamma'_1 = 2\gamma'_e \quad (5.3.4)$$

We note that the relation (5.3.4) can be understood if one re-expresses $\bar{\chi}$ as a function of the elliptic modulus variable $k_<$ in eq. (2.7), since $k_<$ diverges at $u = 1$ with an exponent which is twice as large as the exponent describing its divergence at $u = u_e$, i.e., $k_< \sim (1 - u)^{-1}$ as $u \rightarrow 1$, while $k_< \sim (1 - u/u_e)^{-1/2}$ as $u \rightarrow u_e$.

5.4 Singularity at $u = -1$

We have studied the singularity in $\bar{\chi}$ at $u = -1$ (denoted u_s) by using the series for $\bar{\chi}$ in the variable u and also transforming this series to one in the elliptic modulus variable $k_<$. The series in $k_<$ showed a greater sensitivity to this singularity, and therefore we concentrate on the results from our analysis of this series. The reason for this greater sensitivity is clear; the series in u is strongly affected by the fact that, as one can see from Fig. 2(a), there is an intervening singular line segment protruding into the FM phase and ending at $u = u_e$, in front of the point $u = -1$ as one moves out from the origin along the negative $Re(u)$ axis. The transformation from u to $k_<$ maps the singular endpoint at $u = u_e$ away to $-\infty$ and maps the singularity at $u = 1$ to ∞ in the $k_<$ plane, thereby leaving the singularity at $u = -1$ as the nearest to the origin. Specifically, the image of the singular line segment from $u = u_e$ leftward to $u = -1$ is the semi-infinite line segment from $-\infty$ to -1 in the $k_<$ plane. The line segment from $u = 1/u_e$ to $u = -1$ has the same image, again the segment from $-\infty$ to -1 in the $k_<$ plane, while the unit circle $|u| = 1$ maps to the line segment from 1 to ∞ in this plane. The series in $k_<$ has the form $\bar{\chi} = (1/4)(k_<)^2 \sum_{n=0}^{\infty} c'_n (k_<)^n$, and, as before, we actually analyse the reduced function $\bar{\chi}_r = 4(k_<)^{-2} \bar{\chi}$. Using the Taylor series expansion of $k_<$ near $u = -1$,

$$k_< = -1 - 2^{-5}(1 + u)^4 + O((1 + u)^5) \quad (5.4.1)$$

it follows that as $k_{<} \rightarrow -1$ and $u \rightarrow -1$, the singular form $\bar{\chi} \sim (1 + k_{<})^{-\gamma'_{s,k_{<}}}$ corresponds to $\bar{\chi} \sim (1 + u)^{-\gamma'_s}$, with

$$\gamma'_s = 4\gamma'_{s,k_{<}} \quad (5.4.2)$$

Our results from the differential approximants for this series are given in Table 6 and its continuation. Because the actual pole positions have small imaginary parts, typically a few times 10^{-4} of the size of the real part, there are resultant imaginary parts in the values of the corresponding exponent γ'_s from the differential approximants. Since the exact singularity in $\bar{\chi}(u)$ is at the real value $u = -1$, and since $\bar{\chi}(u, h = i\pi/2)$ is real for real u , we know that γ'_s at $u = (k_{<}) = -1$ is real. Given this and the relation (5.4.2), it follows that we may take only the real parts of the exponents from the differential approximants to the series in $k_{<}$, and we do so.

From this study, we obtain for the position of the singularity

$$(k_{<})_{sing} = -0.9993 \pm 0.0001 \quad (5.4.3)$$

consistent with the expectation $(k_{<})_{sing} = -1$, or equivalently, $u_{sing} = u_s = -1$. As is evident, the values of $Re(\gamma'_s)$ are almost all slightly below 0.25; however, when we carry out our method of plotting the values as a function of the distance $|(k_{<}) + 1|$ and extrapolating to zero distance from the exact singularity, the extrapolated value is actually slightly above 0.25. Accordingly, we give a conservative estimate

$$\gamma'_{s,k_{<}} = 0.250 \pm 0.020 \quad (5.4.4)$$

and hence, using (5.4.2),

$$\gamma'_s = 1.00 \pm 0.08 \quad (5.4.5)$$

This supports the conclusion, which we shall draw, that the exact value of this exponent is

$$\gamma'_s = 1 \quad (5.4.6)$$

We show our summary of exponents in table 8. The exponent relation $\alpha'_{u,ph.} + 2\beta'_u + \gamma'_{u,ph.} = 2$ is evidently satisfied at all three of the singularities $u = u_e$, $u = 1$, and $u = -1$.

6 Extraction and Analysis of Low-Temperature Series for $\bar{\chi}^{(a)}$

We have also investigated the complex-temperature singularities in the staggered susceptibility $\bar{\chi}^{(a)}$ for the present model. To do this, we have extracted and analysed the low-temperature series expansion for this function, using the low-temperature, high staggered

$[L/M_0; M_1]$	$(k_{<})_{sing}$	$ (k_{<})_{sing} + 1 $	$Re(\gamma'_{s,k_{<}})$
[3/6; 7]	$-0.9992689 - 0.0002556i$	7.7×10^{-4}	0.2195
[3/7; 6]	$-0.9992875 - 0.0002801i$	7.7×10^{-4}	0.2204
[3/7; 8]	$-0.9992627 + 0.0004390i$	8.6×10^{-4}	0.2230
[3/7; 9]	$-0.9993572 + 0.0003351i$	7.2×10^{-4}	0.2283
[3/8; 7]	$-0.9992612 + 0.0004332i$	8.6×10^{-4}	0.2228
[3/8; 8]	$-0.9991777 + 0.0000793i$	8.3×10^{-4}	0.2147
[3/9; 7]	$-0.9993502 + 0.0003284i$	7.3×10^{-4}	0.2277
[4/5; 7]	$-0.9992779 - 0.0001344i$	7.3×10^{-4}	0.2205
[4/7; 5]	$-0.9992970 - 0.0001857i$	7.3×10^{-4}	0.2213
[4/7; 8]	$-0.9992847 + 0.0002823i$	7.7×10^{-4}	0.2232
[4/8; 7]	$-0.9992808 + 0.0002780i$	7.7×10^{-4}	0.2229
[5/6; 8]	$-0.9992436 + 0.0002910i$	8.1×10^{-4}	0.2207
[5/7; 7]	$-0.9994218 + 0.0003067i$	6.5×10^{-4}	0.2319
[5/8; 6]	$-0.9992426 + 0.0002845i$	8.1×10^{-4}	0.2206
[6/5; 5]	$-0.9990412 + 0.0000501i$	9.6×10^{-4}	0.2087
[6/6; 6]	$-0.9991672 + 0.0005305i$	9.9×10^{-4}	0.2178
[6/6; 7]	$-0.9994966 + 0.0002217i$	5.5×10^{-4}	0.2368
[6/7; 6]	$-0.9994911 + 0.0002243i$	5.6×10^{-4}	0.2364

Table 6: Values of pole $(k_{<})_{sing}$ near $k_{<} = -1$, i.e. $u = -1$ (denoted u_s), distance from this point, $|(k_{<})_{sing} + 1|$, and real part of exponent, $Re(\gamma'_{s,k_{<}})$ from differential approximants to low-temperature series for $\bar{\chi}_r(k_{<}, h = i\pi/2)$. We list only the approximants which satisfy the accuracy criterion $|(k_{<})_{sing} + 1| < 1 \times 10^{-3}$.

[7/4; 6]	$-1.0004373 + 0.0006097i$	7.5×10^{-4}	0.2916
[7/5; 6]	$-0.9993254 + 0.0004203i$	7.9×10^{-4}	0.2269
[7/5; 7]	$-0.9993665 + 0.0002981i$	7.0×10^{-4}	0.2286
[7/6; 4]	$-0.9998382 + 0.0005474i$	5.7×10^{-4}	0.2573
[7/6; 5]	$-0.9993332 + 0.0004066i$	7.8×10^{-4}	0.2273
[7/6; 6]	$-0.9993588 + 0.0003212i$	7.2×10^{-4}	0.2285
[7/7; 5]	$-0.9993650 + 0.0003025i$	7.0×10^{-4}	0.2286
[8/4; 6]	$-0.9993815 + 0.0001580i$	6.4×10^{-4}	0.2286
[8/5; 6]	$-0.9993680 + 0.0002999i$	7.0×10^{-4}	0.2287
[8/6; 4]	$-0.9993746 + 0.0002485i$	6.7×10^{-4}	0.2288
[8/6; 5]	$-0.9993660 + 0.0003035i$	7.0×10^{-4}	0.2287
[9/4; 5]	$-0.9992599 + 0.0000684i$	7.4×10^{-4}	0.2199
[9/4; 6]	$-1.0005762 + 0.0005457i$	7.9×10^{-4}	0.3106
[9/5; 4]	$-0.9992690 + 0.0001240i$	7.4×10^{-4}	0.2209
[9/5; 5]	$-0.9992719 + 0.0002258i$	7.6×10^{-4}	0.2218
[9/6; 4]	$-0.9995104 + 0.0003921i$	6.3×10^{-4}	0.2390
[10/4; 4]	$-0.9994550 - 0.0001668i$	5.7×10^{-4}	0.2311
[10/4; 5]	$-0.9991991 + 0.0001605i$	8.2×10^{-4}	0.2164
[10/5; 4]	$-0.9992330 + 0.0001856i$	7.9×10^{-4}	0.2189

Table 7: Continuation of table of differential approximants for $\bar{\chi}_r$ series in the variable $k_<$ near $u = k_< = -1$.

u	$\alpha'_{u,FM}$	$\alpha'_{u,AFM}$	β_u	γ'_u	$\alpha'_{u,ph.} + 2\beta'_u + \gamma'_{u,ph.}$
$u_e = -(3 - 2^{3/2})$	1	—	$-1/8$	$5/4$	2
1	0 finite*	0 finite*	$-1/4$	$5/2$	2
$u_s = -1$	0 finite	0 finite	$1/2$	1	2

Table 8: Exponents at singularities in the 2D Ising model with $h = \pm i\pi/2$. The results for α'_u and β_u are exact; the results for γ'_u are our conclusions for the exact values from our series analysis. The notation — indicates that the point cannot be approached from within the given phase. For the singularity of C at $u = 1$ (marked with a *), the values of α' correspond to evaluating $K = -(1/4)\ln(1) = 0$ on the principal Riemann sheet of the logarithm, as discussed in the text.

field series expansions for the free energy of the Ising model on the square lattice calculated by the King's College group [30, 25]. These are denoted antiferromagnetic polynomials in these papers and were calculated to order $O(w^{11})$ in Ref. [25], where, as before, $w = 1/u$ is the low-temperature expansion variable in the AFM phase. The antiferromagnetic polynomials were apparently not calculated to higher order subsequently [31]. We have extracted from these the resultant low-temperature series expansion for $\bar{\chi}^{(a)}$ for $h = i\pi/2$, which is

$$\begin{aligned} \bar{\chi}^{(a)}(h = i\pi/2) = 4w^2 & \left[-1 - 8w^2 + 24w^3 - 135w^4 + 648w^5 - 3336w^6 \right. \\ & \left. + 17240w^7 - 90501w^8 + 479192w^9 + O(w^{10}) \right] \end{aligned} \quad (6.1)$$

For reference, we recall that the series for $\bar{\chi}^{(a)}$ for $h = 0$ on this lattice is [30, 25]

$$\bar{\chi}^{(a)}(h = 0) = 4w^2 \left[1 + 4w^2 + 8w^3 + 39w^4 + 152w^5 + 672w^6 + 3016w^7 + 13989w^8 + 66664w^9 + O(w^{10}) \right] \quad (6.2)$$

The series (6.1) is much shorter than the one which we extracted for $\bar{\chi}$, given by eq. (5.1.2) and Table 1, and hence one does not expect to derive results for $\bar{\chi}^{(a)}$ which are as precise as those which we obtained for $\bar{\chi}$. As before, we have used both dlog Padé and differential approximants for this analysis.

We study first the vicinity of the singular point $w = 1$. In Table 9 we list the pole locations and resultant exponents for the approximants which satisfy the accuracy requirement $|w_{sing} - 1| \leq 0.05$. One would not normally expect a dlog Padé approximant of such low order as $[1/2]$ to yield an accurate result; however, it happens that the denominator of this approximant is $\propto (1 - w)(1 - (11/2)w)$, so that it produces a location for the pole which is exact. For this reason, it yields a much better determination of the associated exponent than would otherwise have been the case. This fortuitously accurate approximant, and the best differential approximant, $[3/2; 2]$, both give $\gamma'_{1,a}$ values of about 2.5. From the full set, we infer the crude result

$$\gamma'_{1,a} = 2.5 \pm 0.5 \quad (6.3)$$

This is consistent with the exact value $\gamma'_{1,a} = 5/2$ and hence with the equality $\gamma'_{1,a} = \gamma'_1$. However, clearly the results for $\gamma'_{1,a}$ are much less precise than our determination of γ'_1 .

We also studied the series in the vicinity of the singular endpoint $w = w_e = -(3 - 2^{3/2})$ (i.e., $u = u_{oe} = 1/u_e = -(3 + 2^{3/2})$). To optimise the sensitivity, we calculated and analysed series in transformed variables to map the singularity at $w = 1$ away. We required these variables to be equal to w for small w and to map $w = \pm\infty$ to $\pm\infty$, respectively. Two such variables were $w' = w(1 + w/8)(1 - w)^{-1}$ and $w'' = w(1 - w)^{-1} \sinh w$. The series in the transformed variables did slightly better in locating the pole positions in w'_e and w''_e corresponding to w_e . The dlog Padé and differential approximants indicated that $\bar{\chi}^{(a)}$ has a

PA or DA	w_{sing}	$ w_{sing} - 1 $	$\gamma'_{1,a}$
[1/2]	1	0	2.462
[2/3]	1.04562	4.6×10^{-2}	2.626
[2/4]	0.950447	5.0×10^{-2}	2.063
[4/4]	0.956193	4.4×10^{-2}	2.063
[3/5]	0.969809	3.0×10^{-2}	2.162
[0/3; 4]	0.955169	4.5×10^{-2}	2.057
[0/4; 2]	0.955792	4.4×10^{-2}	2.172
[2/2; 2]	0.999046	0.95×10^{-3}	2.554
[3/2; 2]	0.952282	4.8×10^{-2}	2.357

Table 9: Values of pole near $w = 1$ (denoted w_1), normalised distance from this point, $|w_{sing} - 1|$, and exponent $\gamma'_{1,a}$ from dlog Padé and differential approximants to low-temperature series for $\bar{\chi}_r^{(a)}$. We list only the Padé and differential approximants which satisfy the accuracy criterion $|w_{sing} - 1| \leq 0.05$.

divergent singularity at w_e and yielded values for the associated exponent $\gamma'_{oe,a}$ in the range from about 0.2 to 0.4. Given our exact results $\alpha'_{oe} = 1$ for the specific heat and $\beta_{oe} = -1/4$ for the staggered magnetisation, a value within the above range for $\gamma'_{oe,a}$ would indicate a violation of the exponent relation $\alpha'_{oe} + 2\beta_{oe} + \gamma'_{oe} = 2$. In this context, it is of interest to note that we have already found violations of the relation $\alpha + 2\beta + \gamma = 2$ at complex-temperature singularities, e.g., in the zero-field Ising model on the square lattice at $u = u_s = -1$, as approached from within the PM phase, where $\alpha_s = 0$, $\beta_s = 1/4$, and $\gamma_s < 0$ (since $\bar{\chi}$ has a finite non-analyticity for the approach from within the PM phase) [18], and in the zero-field Ising model on the honeycomb lattice, at the point $z = z_\ell = -1$, as approached from within the FM phase, where $\alpha'_\ell = 2$, $\beta_\ell = -1/4$, and $\gamma'_\ell = 5/2$, so that $\alpha'_\ell + 2\beta_\ell + \gamma'_\ell = 4$ [20].

7 Complex-Temperature Behaviour of the Correlation Length

In this section we shall study the complex-temperature behaviour of the correlation length. To do this, we make use of a calculation of the asymptotic form of the spin-spin correlation function along a row (or equivalently, column), $\langle \sigma_{0,0} \sigma_{n,0} \rangle$, for large n [5] (where, without loss of generality, one may take $n > 0$). From this calculation, carrying out an analytic

continuation to complex temperature, we obtain, for $n \rightarrow \infty$,

$$\begin{aligned} \langle \sigma_{0,0} \sigma_{n,0} \rangle_{conn.} &\sim -(2/\pi)(1-u^2)^{-1} M^2 n^{-1} u(-u)^n \\ &= -(2/\pi)(1-u)^{-3/2}(1+6u+u^2)^{-1/4} n^{-1} u(-u)^n \end{aligned} \quad (7.1)$$

where we have used the exact expression for M , (4.1). This analytic continuation applies within the FM phase. Extracting the correlation length ξ in the usual way as $\xi^{-1} = -\lim_{r \rightarrow \infty} r^{-1} \ln(\langle \sigma_{\mathbf{0}} \sigma_{\mathbf{r}} \rangle_{conn.})$, where $r \equiv |\mathbf{r}|$, we find

$$\xi_{row}^{-1} = -\ln(-u) \quad (7.2)$$

For usual physical second-order critical points, one can use the connected 2-spin correlation function for any \mathbf{r} , with $|\mathbf{r}| \rightarrow \infty$, to extract the correlation length ξ . However, in our previous work [18, 19], we found that at the complex-temperature singular point $u = u_s = -1$ in the zero-field Ising model on the square lattice, the correlation length defined from the diagonal connected 2-spin correlation function diverges with a different exponent, $\nu'_{s,diag} = 2$, than the exponent $\nu'_s = 1$ describing the divergence in the correlation length defined from off-diagonal (e.g., row) correlation functions. In view of this, we include the suffix *row* in (7.2) for clarity. We now consider three particular singular points which can be approached from within the complex-temperature FM phase, viz., $u = u_e$, $u = -1$, and $u = 1$. As $u \rightarrow u_e$, the 2-spin correlation function (7.1) diverges, like $(1 - u/u_e)^{-1/4}$, because of the divergence in the prefactor M^2 , but the correlation length ξ_{row} remains finite, with $\xi_{row}^{-1} = -\ln(-u_e) = 1.7627\dots$ at $u = u_e$. If this feature of a finite correlation length applied to all of the connected 2-spin correlation functions, precisely at $u = u_e$ as well as for points approaching u_e from within the complex-temperature FM phase, then by the same argument as was used in Ref. [8], it would follow that the only singularity in $\bar{\chi}$ would arise from the divergent M^2 prefactor.³ We know, however, that the above premise cannot be true, since then the susceptibility exponent at u_e (as approached from within the FM phase) would be 1/4, whereas we found that $\gamma'_e = 5/4$. The fact that the susceptibility diverges with an exponent different from that arising from the divergent M^2 prefactor shows that at least some connected 2-spin correlation functions must decay like a power law, i.e. the associated correlation length must be divergent, at $u = u_e$. To get more information on this, it would be useful to carry out analytic calculations of the asymptotic forms of the general 2-spin correlation functions $\langle \sigma_{0,0} \sigma_{m,n} \rangle$ in the present model, near to and at this singular point.

³Define $\langle \sigma_{\mathbf{0}} \sigma_{\mathbf{r}} \rangle = M^2 c(\mathbf{r})$. Then $\bar{\chi} = M^2 \sum_{\mathbf{r}} c(\mathbf{r})$. For purposes of analysing divergences, the asymptotic behaviour of the sum can be approximated by that of the integral $\int d^2r c(\mathbf{r})$ for large r (with a short-distance cutoff on the latter). If $c(\mathbf{r}) \sim r^{-p} e^{-r/\xi}$ as $r \rightarrow \infty$, this integral is finite. Therefore, a divergence in $\bar{\chi}$ would arise solely from a divergence in the prefactor M^2 . This was noted in Ref. [19].

As $u \rightarrow 1$, the 2-spin correlation function (7.1) again diverges, like $(1 - u)^{-3/2}$, and the correlation length ξ_{row} is finite: $\xi_{row}^{-1} = -\ln(-1) = -i\pi$ (for the principal Riemann sheet of the logarithm). This is a case similar that discussed in [8] where $Re(\xi^{-1}) = 0$ but $Im(\xi^{-1}) \neq 0$.

As $u \rightarrow -1$, each 2-spin correlation function is finite, but the correlation length does diverge, with exponent

$$\nu'_s = 1 \tag{7.3}$$

If one were to use the exponent relation $\gamma'_s = \nu'_s(2 - \eta_s)$, then with our inference $\gamma'_s = 1$ in eq. (5.4.6), it would follow that $\eta_s = 1$. However, we have shown previously [18] that one must use caution in trying to apply such exponent relations at complex-temperature singularities, since different connected spin-spin correlation functions may be characterised by correlation lengths which diverge with different exponents ν .

This type of analysis can also be done with the staggered 2-spin correlation functions (c.f. (4.11))

$$\langle \tilde{\sigma}_{0,0} \tilde{\sigma}_{n,0} \rangle_{conn.} = (-1)^n \langle \sigma_{0,0} \sigma_{n,0} \rangle_{conn.} \tag{7.4}$$

In particular, as $u \rightarrow 1/u_e$ (i.e., $w \rightarrow w_e$), these correlation functions diverge, like $(1 - w/w_e)^{-1/4}$, because of the divergent prefactor M_{st}^2 . However, the correlation length $\xi_{row,AFM}$ remains finite. If this behaviour characterised all of the staggered 2-spin correlation functions, at w_e as well as in the vicinity of w_e , then the only divergence in $\bar{\chi}^{(a)}$ would arise from the M_{st}^2 prefactor, and hence $\gamma'_{e,a} = 1/4$. This value is consistent with our results from the analysis of the low-temperature series for $\bar{\chi}^{(a)}$. This merits further study.

8 Exact Solution at $u = 1$ for Arbitrary H

In the body of this paper, we have investigated singularities in the square lattice Ising model as functions of complex-temperature, for the fixed value of external magnetic field, $h = i\pi/2$ (or $h = -i\pi/2$). It is also of interest to study the complementary problem of singularities as a function of h for fixed K or u . Indeed, in pursuing such a study, Yang and Lee were led to their celebrated circle theorem on the zeros of the partition function for the Ising model in the complex e^{2h} plane [1, 32]. Here, we would like to mention some elementary results which elucidate how various quantities become singular at a particularly simple point, $u = 1$, as h is varied. These results may be combined with our determination of the exact singularities in f , U , C , and M as one approaches this point by varying u . At $J = 0$, hence $K = 0$ and $u = 1$, the partition function reduces to a single-site problem, which can easily be calculated exactly for arbitrary H , dimensionality, and lattice type. We find, independent

of the dimensionality and lattice type,

$$f(u = 1, h) = \ln(2 \cosh h) \quad (8.1)$$

$$U = -H \tanh h \quad (8.2)$$

$$k_B^{-1} C = \frac{h^2}{\cosh^2 h} \quad (8.3)$$

$$M = \tanh h \quad (8.4)$$

$$\bar{\chi} = \frac{1}{\cosh^2 h} \quad (8.5)$$

Further, the m -point correlation functions factorise trivially and are independent of the positions of the spins:

$$\langle \sigma_{\mathbf{r}_1} \cdots \sigma_{\mathbf{r}_m} \rangle = \langle \sigma_{\mathbf{r}_1} \rangle^m = M^m = (\tanh h)^m \quad (8.6)$$

To study the singularities of these functions, we must define new exponents, since the usual critical exponents apply to singularities of thermodynamic quantities as functions of T . To avoid a profusion of new symbols, we shall use the same Greek letters as for the respective T -dependent singularities in thermodynamic quantities, but use a superscript (h) to indicate that they describe the singularity as a function of h for $K = 0$. Thus, for the leading singularity in the specific heat, as a function of h , at the point $h = h_s$ (s denotes a generic singularity here) for fixed $K = 0$ (hence $u = 1$), we shall write

$$C(h)_{sing.} \sim A_{C,s,dir.}^{(h)} (h - h_s)^{-\alpha_{s,dir.}^{(h)}} \quad (8.7)$$

where $dir.$ denotes the direction, in the complex h plane, from which one approaches the singular point h_s . Similarly, we shall write

$$\chi_{sing.} \sim A_{\chi,s,dir.}^{(h)} (h - h_s)^{\gamma_{s,dir.}^{(h)}} \quad (8.8)$$

and so forth for the singularities in other quantities. From (8.3), it is evident that C diverges for

$$h = (2n + 1) \frac{i\pi}{2}, \quad n \in Z \quad (8.9)$$

with corresponding exponent

$$\alpha_1^{(h)} = 2 \quad (8.10)$$

for any direction of approach to any of the singular points (8.9). The internal energy itself also diverges at these points, with the exponent $\alpha_1^{(h)} - 1 = 1$ and vanishes at the set

$$h = ni\pi, \quad n \in Z \quad (8.11)$$

The magnetisation vanishes and diverges at the same set of points as the internal energy U (c.f. eqs. (8.11) and (8.9) with the respective exponents

$$\beta_{1,zero}^{(h)} = 1 \quad (8.12)$$

and

$$\beta_{1,div}^{(h)} = -1 \quad (8.13)$$

again, independent of the direction of approach to these points in the complex h plane. The susceptibility diverges at the points (8.9) with exponent

$$\gamma_1^{(h)} = 2 \quad (8.14)$$

It is useful to evaluate the general results above for the interesting special case of complex $h = h_r + i\pi/2$ where h_r is real. For this case, we have

$$f = \ln(2i \sinh h_r) \quad (8.15)$$

$$U = -\frac{H}{\tanh h_r} \quad (8.16)$$

$$k_B^{-1}C = -\frac{(h_r + i\pi/2)^2}{\sinh^2 h_r} \quad (8.17)$$

$$M = \frac{1}{\tanh h_r} \quad (8.18)$$

$$\bar{\chi} = -\frac{1}{\sinh^2 h_r} \quad (8.19)$$

and

$$\langle \sigma_{\mathbf{r}_1} \cdots \sigma_{\mathbf{r}_m} \rangle = (\tanh h_r)^{-m} \quad (8.20)$$

As $h_r \rightarrow 0$ so that $h \rightarrow i\pi/2$, we recover our previous results, that U and M diverge linearly while C and $\bar{\chi}$ diverge quadratically.

For loose-packed lattices, it is straightforward to extend these results to consider a staggered rather than uniform external field, H_{st} , i.e. to consider the partition function

$$Z = \sum_{\{\sigma_n\}} \exp\left(\sum_n (-1)^{p(n)} h_{st} \sigma_n\right) \quad (8.21)$$

where $p(n)$ was defined in eq. (4.12) and $h_{st} = \beta H_{st}$. Since the summations over the spins on the even and odd sublattices are decoupled, one finds the same equations as before, but with H replaced by H_{st} , i.e., $f = \ln(2 \cosh h_{st})$, $U = -H_{st} \tanh h_{st}$, $C = k_B h_{st}^2 / \cosh^2 h_{st}$, and $M_{st} = \tanh h_{st}$. The staggered susceptibility is $\bar{\chi}^{(a)} = 1 / \cosh^2 h_{st}$.

9 Conclusions

In this paper, we have studied a natural generalisation of an exactly solved model from real non-negative temperature to complex temperature. This is the Ising model on the square lattice in an external magnetic field given by $\beta H = \pm i\pi/2$, first solved by Lee and Yang [1]. We have worked out the complex-temperature phase boundaries, as shown in Fig. 2. We have also extracted a low-temperature series expansion for the susceptibility, $\bar{\chi}$. From an analysis of this series using dlog Padé and differential approximants, we conclude that $\bar{\chi}$ has divergent singularities at $u = u_e = -(3 - 2^{3/2})$ with exponent $\gamma'_e = 5/4$, at $u = 1$ with exponent $\gamma'_1 = 5/2$, and at $u = u_s = -1$ with exponent $\gamma'_s = 1$. We have also studied the staggered susceptibility. Using exact results, we have determined the complex-temperature singularities of the specific heat and the uniform and staggered magnetisation. We are currently in the process of extending our studies to other 2D lattices. The findings show again that even though the Ising model has a very simple Hamiltonian, it exhibits a fascinating richness of properties.

This research was supported in part by the NSF grant PHY-93-09888. One of us (R.S.) thanks Prof. C. N. Yang for a discussion of Ref. [1] and Profs. D. S. Gaunt and A. J. Guttmann for discussions of the current status of low-temperature series expansions.

References

- [1] Lee, T. D. and Yang, C. N. 1952 *Phys. Rev.* **87** 410.
- [2] Onsager, L. 1944 *Phys. Rev.* **65** 117.
- [3] Yang, C. N. 1952 *Phys. Rev.* **85** 808.
- [4] Baxter, G. 1965 *J. Math. Phys.* **6** 1015; 1966 *J. Math. Phys.* **8** 399.
- [5] McCoy, B. and Wu, T. T. 1967 *Phys. Rev.* **155** 438.
- [6] Merlini, D. 1974 *Lett. Nuovo Cim.* **9** 100.
- [7] Lin, K. Y. and Wu, F. Y. 1988 *Int. J. Mod. Phys. B* **4** 471.
- [8] Marchesini, G. and Shrock, R. E. 1989 *Nucl. Phys. B* **318** 541.
- [9] Utiyama, T. 1951 *Prog. Theor. Phys.* **6** 907.
- [10] Syozi, I. and Naya, S. 1960 *Prog. Theor. Phys.* **23** 374; *ibid.* **24** 829.
- [11] Baxter, R. J. 1986 *Proc. Roy. Soc. Lond.* **A404** 1.
- [12] Fisher, M. E. 1965 *Lectures in Theoretical Physics* (Univ. of Colorado Press, Boulder), vol. 12C, p. 1.
- [13] Thompson, C. J., Guttmann, A. J., Ninham, B. W. 1969 *J. Phys. C* **2** 1889; Guttmann, A. J. 1969 *ibid*, 1900.
- [14] Domb, C. and Guttmann, A. J. 1970 *J. Phys. C* **3** 1652.
- [15] Guttmann, A. J. 1975 *J. Phys. A: Math. Gen.* **8** 1236.
- [16] Itzykson, C., Pearson, R., and Zuber, J.B. 1983 *Nucl. Phys. B* **220** 415.
- [17] Enting, I. G., Guttmann, A. J., and Jensen, I. 1994 *J. Phys. A: Math. Gen.* **27** 6963.
- [18] Matveev, V. and Shrock, R., “Complex-Temperature Singularities of the Susceptibility in the $d = 2$ Ising Model. I. Square Lattice” ITP-SB-94-37 (Aug. 1994) (hep-lat/9408020), *J. Phys. A: Math. Gen.*, in press.
- [19] Matveev, V. and Shrock, R., “Complex-Temperature Singularities in the $d = 2$ Ising Model. II. Triangular Lattice” ITP-SB-94-53 (Nov. 1994) (hep-lat/9411023), submitted to *J. Phys. A: Math. Gen.*.

- [20] Matveev, V. and Shrock, R., “Complex-Temperature Singularities in the $d = 2$ Ising Model. III. Honeycomb Lattice” ITP-SB-9454 (Dec. 1994) (hep-lat/9412076), submitted to *J. Phys. A: Math. Gen.*.
- [21] Gradshteyn, I. and Ryzhik, I. 1980 *Table of Integrals, Series, and Products* (Academic, New York), eq. 8.126.3.
- [22] Kaufmann, B. and Onsager, L. 1949 *Phys. Rev.* **76** 1244.
- [23] Montroll, E. W., Potts, R. B., and Ward, J. C. 1963 *J. Math. Phys.* **4** 308.
- [24] Ghosh, R. K. and Shrock, R. E. 1984 *Phys. Rev. B* **30** 3790; 1985 *J. Stat. Phys.* **38** 473; 1985 *Phys. Rev. B* **31** 1486.
- [25] Sykes, M. F., Gaunt, D. S., Martin, J. L, Mattingly, S. R., and Essam, J. W. 1973 *J. Math. Phys. A: Math. Gen.* **14** 1071.
- [26] Sykes, Watts, M. G., and Gaunt, D. S. 1975 *J. Math. Phys. A: Math. Gen.* **8** 1448.
- [27] Baxter, R. J. and Enting, I. G. 1979 *J. Stat. Phys.* **21** 103.
- [28] Briggs, K. M., Enting, I. G., and Guttmann, A. J. 1994 *J. Phys. A: Math. Gen.* **27** 1503 (hep-lat/9312082).
- [29] Guttmann, A. J. 1989 in *Phase Transitions and Critical Phenomena*, Domb, C. and Lebowitz, J., eds. (Academic Press, New York) vol. 13.
- [30] Sykes, M. F., Essam, J. W., Gaunt, D. S. 1965 *J. Math. Phys.* **6** 283 and references therein.
- [31] Gaunt, D. S. 1994 private communication.
- [32] Yang, C. N. and Lee, T. D. 1952 *Phys. Rev.* **87** 404.

Appendix

Here we list our differential approximant results relevant for the singularity in $\bar{\chi}(u, h = i\pi/2)$ at $u = u_e$.

$[L/M_0; M_1]$	u_{sing}	$ u_{sing} - u_e / u_e $	γ'_e
[0/4; 6]	-0.1715614	6.7×10^{-5}	1.2455
[0/5; 5]	-0.1715743	8.1×10^{-6}	1.2474
[0/5; 6]	-0.1715716	7.2×10^{-6}	1.2470
[0/5; 7]	-0.1715696	1.9×10^{-5}	1.2467
[0/6; 4]	-0.1715688	2.4×10^{-5}	1.2466
[0/6; 5]	-0.1715717	6.6×10^{-6}	1.2470
[0/6; 7]	-0.1715661	3.9×10^{-5}	1.2461
[0/6; 8]	-0.1715659	4.1×10^{-5}	1.2460
[0/7; 5]	-0.1715706	1.3×10^{-5}	1.2469
[0/7; 6]	-0.1715662	3.9×10^{-5}	1.2461
[0/7; 7]	-0.1715659	4.1×10^{-5}	1.2460
[0/7; 8]	-0.1715660	4.0×10^{-5}	1.2460
[0/7; 9]	-0.1715628	5.8×10^{-5}	1.2456
[0/8; 6]	-0.1715658	4.1×10^{-5}	1.2460
[0/8; 7]	-0.1715660	4.0×10^{-5}	1.2460
[0/8; 8]	-0.1715654	4.3×10^{-5}	1.2459
[0/8; 10]	-0.1715690	2.2×10^{-5}	1.2469
[0/9; 7]	-0.1715599	7.6×10^{-5}	1.2456
[0/9; 8]	-0.1715549	1.0×10^{-4}	1.2468
[0/9; 9]	-0.1715754	1.5×10^{-5}	1.2505
[0/9; 10]	-0.1715716	7.2×10^{-6}	1.2481
[0/10; 8]	-0.1715584	8.5×10^{-5}	1.2456
[0/10; 9]	-0.1715718	6.4×10^{-6}	1.2482
[1/5; 5]	-0.1715621	6.3×10^{-5}	1.2449
[1/5; 6]	-0.1715609	7.0×10^{-5}	1.2447
[1/5; 7]	-0.1715625	6.0×10^{-5}	1.2450
[1/6; 5]	-0.1715609	7.0×10^{-5}	1.2446
[1/6; 6]	-0.1715615	6.7×10^{-5}	1.2448
[1/6; 7]	-0.1715649	4.7×10^{-5}	1.2457
[1/6; 8]	-0.1715676	3.1×10^{-5}	1.2466
[1/7; 5]	-0.1715624	6.1×10^{-5}	1.2450
[1/7; 6]	-0.1715647	4.8×10^{-5}	1.2457

Table 10: Values of pole near $u_e = -(3 - 2^{3/2}) = -0.171572876\dots$, normalised distance from this point, $|u_{sing} - u_e|/|u_e|$, and exponent γ'_e from differential approximants (DA's) to low-temperature series for $\bar{\chi}_r$. We list only the differential approximants which satisfy the accuracy criterion $|u_{sing} - u_e|/|u_e| \leq 1 \times 10^{-4}$.

[1/7; 7]	-0.1715669	3.5×10^{-5}	1.2463
[1/7; 8]	-0.1715682	2.7×10^{-5}	1.2468
[1/7; 9]	-0.1715702	1.6×10^{-5}	1.2475
[1/8; 6]	-0.1715676	3.1×10^{-5}	1.2466
[1/8; 7]	-0.1715682	2.7×10^{-5}	1.2468
[1/8; 8]	-0.1715690	2.2×10^{-5}	1.2471
[1/8; 9]	-0.1715700	1.7×10^{-5}	1.2474
[1/8; 10]	-0.1715701	1.6×10^{-5}	1.2475
[1/9; 7]	-0.1715769	2.4×10^{-5}	1.2513
[1/9; 8]	-0.1715699	1.7×10^{-5}	1.2474
[1/9; 9]	-0.1715704	1.4×10^{-5}	1.2476
[1/10; 8]	-0.1715702	1.5×10^{-5}	1.2475
[2/4; 4]	-0.1715557	1.0×10^{-4}	1.2435
[2/4; 5]	-0.1715555	1.0×10^{-4}	1.2434
[2/4; 6]	-0.1715609	7.0×10^{-5}	1.2446
[2/5; 4]	-0.1715555	1.0×10^{-4}	1.2434
[2/5; 5]	-0.1715609	7.0×10^{-5}	1.2446
[2/5; 6]	-0.1715612	6.8×10^{-5}	1.2445
[2/5; 7]	-0.1715651	4.5×10^{-5}	1.2460
[2/6; 4]	-0.1715609	7.0×10^{-5}	1.2446
[2/6; 5]	-0.1715612	6.8×10^{-5}	1.2446
[2/6; 6]	-0.1715671	3.4×10^{-5}	1.2479
[2/6; 7]	-0.1715658	4.2×10^{-5}	1.2466
[2/6; 8]	-0.1715686	2.5×10^{-5}	1.2466
[2/7; 5]	-0.1715649	4.6×10^{-5}	1.2459
[2/7; 6]	-0.1715657	4.2×10^{-5}	1.2467
[2/7; 7]	-0.1715701	1.6×10^{-5}	1.2463
[2/7; 8]	-0.1715688	2.4×10^{-5}	1.2465
[2/7; 9]	-0.1715698	1.8×10^{-5}	1.2473
[2/8; 6]	-0.1715685	2.6×10^{-5}	1.2466
[2/8; 7]	-0.1715688	2.4×10^{-5}	1.2465
[2/8; 8]	-0.1715686	2.5×10^{-5}	1.2459
[2/8; 9]	-0.1715737	4.5×10^{-6}	1.2501
[2/9; 7]	-0.1715693	2.1×10^{-5}	1.2468
[2/9; 8]	-0.1715785	3.3×10^{-5}	1.2506
[3/4; 4]	-0.1715556	1.0×10^{-4}	1.2434
[3/4; 5]	-0.1715619	6.4×10^{-5}	1.2449
[3/4; 6]	-0.1715632	5.6×10^{-5}	1.2452

Table 11: Continuation of DA Table for u_e Singularity.

[3/5; 3]	-0.1715648	4.7×10^{-5}	1.2455
[3/5; 4]	-0.1715616	6.6×10^{-5}	1.2448
[3/5; 5]	-0.1715628	5.8×10^{-5}	1.2451
[3/5; 6]	-0.1715657	4.2×10^{-5}	1.2460
[3/5; 7]	-0.1715672	3.3×10^{-5}	1.2463
[3/6; 4]	-0.1715637	5.3×10^{-5}	1.2454
[3/6; 5]	-0.1715656	4.2×10^{-5}	1.2460
[3/6; 6]	-0.1715660	4.0×10^{-5}	1.2466
[3/6; 7]	-0.1715689	2.3×10^{-5}	1.2463
[3/6; 8]	-0.1715687	2.4×10^{-5}	1.2464
[3/7; 5]	-0.1715672	3.3×10^{-5}	1.2463
[3/7; 6]	-0.1715690	2.3×10^{-5}	1.2463
[3/7; 7]	-0.1715686	2.5×10^{-5}	1.2463
[3/7; 8]	-0.1715699	1.7×10^{-5}	1.2478
[3/7; 9]	-0.1715697	1.9×10^{-5}	1.2464
[3/8; 6]	-0.1715687	2.4×10^{-5}	1.2464
[3/8; 7]	-0.1715696	1.9×10^{-5}	1.2474
[3/8; 8]	-0.1715619	6.4×10^{-5}	1.2297
[3/9; 7]	-0.1715680	2.8×10^{-5}	1.2436
[4/4; 3]	-0.1715679	2.9×10^{-5}	1.2462
[4/4; 4]	-0.1715608	7.0×10^{-5}	1.2446
[4/4; 5]	-0.1715630	5.7×10^{-5}	1.2452
[4/4; 6]	-0.1715669	3.5×10^{-5}	1.2464
[4/5; 3]	-0.1715628	5.9×10^{-5}	1.2451
[4/5; 4]	-0.1715632	5.6×10^{-5}	1.2452
[4/5; 5]	-0.1715648	4.7×10^{-5}	1.2458
[4/5; 6]	-0.1715670	3.4×10^{-5}	1.2465
[4/5; 7]	-0.1715686	2.5×10^{-5}	1.2454
[4/6; 4]	-0.1715663	3.8×10^{-5}	1.2462
[4/6; 5]	-0.1715673	3.2×10^{-5}	1.2464
[4/6; 6]	-0.1715689	2.3×10^{-5}	1.2465
[4/6; 7]	-0.1715690	2.3×10^{-5}	1.2468
[4/6; 8]	-0.1715635	5.5×10^{-5}	1.2360
[4/7; 5]	-0.1715685	2.5×10^{-5}	1.2480
[4/7; 6]	-0.1715689	2.3×10^{-5}	1.2466
[4/7; 7]	-0.1715770	2.4×10^{-5}	1.2503
[4/7; 8]	-0.1715900	1.0×10^{-4}	1.2273
[4/8; 6]	-0.1715674	3.2×10^{-5}	1.2441

Table 12: Continuation of DA Table for u_e Singularity.

[5/4; 3]	-0.1715611	6.9×10^{-5}	1.2446
[5/4; 4]	-0.1715611	6.9×10^{-5}	1.2446
[5/4; 5]	-0.1715654	4.4×10^{-5}	1.2459
[5/4; 6]	-0.1715670	3.4×10^{-5}	1.2465
[5/5; 3]	-0.1715607	7.1×10^{-5}	1.2445
[5/5; 4]	-0.1715653	4.4×10^{-5}	1.2459
[5/5; 5]	-0.1715674	3.2×10^{-5}	1.2462
[5/5; 6]	-0.1715754	1.4×10^{-5}	1.2488
[5/5; 7]	-0.1715682	2.7×10^{-5}	1.2456
[5/6; 4]	-0.1715673	3.3×10^{-5}	1.2465
[5/6; 5]	-0.1715662	3.9×10^{-5}	1.2490
[5/6; 6]	-0.1715688	2.4×10^{-5}	1.2466
[5/6; 8]	-0.1715835	6.2×10^{-5}	1.2433
[5/7; 5]	-0.1715698	1.8×10^{-5}	1.2478
[5/7; 6]	-0.1715665	3.7×10^{-5}	1.2427
[5/7; 7]	-0.1715882	8.9×10^{-5}	1.2325
[5/8; 6]	-0.1715723	3.5×10^{-6}	1.2495
[6/4; 2]	-0.1715686	2.5×10^{-5}	1.2473
[6/4; 3]	-0.1715610	6.9×10^{-5}	1.2446
[6/4; 4]	-0.1715642	5.1×10^{-5}	1.2455
[6/4; 5]	-0.1715667	3.6×10^{-5}	1.2463
[6/4; 6]	-0.1715683	2.7×10^{-5}	1.2472
[6/5; 3]	-0.1715655	4.3×10^{-5}	1.2459
[6/5; 4]	-0.1715666	3.6×10^{-5}	1.2463
[6/5; 5]	-0.1715697	1.9×10^{-5}	1.2464
[6/5; 6]	-0.1715689	2.3×10^{-5}	1.2468
[6/5; 7]	-0.1715662	3.9×10^{-5}	1.2420
[6/6; 4]	-0.1715685	2.5×10^{-5}	1.2469
[6/6; 5]	-0.1715689	2.3×10^{-5}	1.2467
[6/6; 6]	-0.1715686	2.5×10^{-5}	1.2460
[6/6; 7]	-0.1715819	5.3×10^{-5}	1.2461
[6/7; 5]	-0.1715630	5.8×10^{-5}	1.2355
[6/7; 6]	-0.1715746	9.9×10^{-6}	1.2505
[7/4; 2]	-0.1715853	7.2×10^{-5}	1.2519
[7/4; 3]	-0.1715648	4.7×10^{-5}	1.2457
[7/4; 4]	-0.1715679	2.9×10^{-5}	1.2466
[7/4; 5]	-0.1715679	2.9×10^{-5}	1.2466
[7/4; 6]	-0.1715707	1.3×10^{-5}	1.2495

Table 13: Continuation of DA Table for u_e Singularity.

[7/5; 3]	-0.1715664	3.8×10^{-5}	1.2462
[7/5; 4]	-0.1715679	2.9×10^{-5}	1.2466
[7/5; 5]	-0.1715687	2.4×10^{-5}	1.2464
[7/5; 6]	-0.1715678	2.9×10^{-5}	1.2446
[7/5; 7]	-0.1715709	1.2×10^{-5}	1.2483
[7/6; 4]	-0.1715691	2.2×10^{-5}	1.2471
[7/6; 5]	-0.1715672	3.3×10^{-5}	1.2433
[7/6; 6]	-0.1715652	4.5×10^{-5}	1.2388
[7/7; 5]	-0.1715689	2.3×10^{-5}	1.2458
[8/4; 2]	-0.1715791	3.6×10^{-5}	1.2505
[8/4; 3]	-0.1715670	3.4×10^{-5}	1.2464
[8/4; 4]	-0.1715679	2.9×10^{-5}	1.2466
[8/4; 5]	-0.1715683	2.7×10^{-5}	1.2465
[8/4; 6]	-0.1715609	7.0×10^{-5}	1.2283
[8/5; 3]	-0.1715677	3.0×10^{-5}	1.2467
[8/5; 4]	-0.1715682	2.7×10^{-5}	1.2465
[8/5; 5]	-0.1715691	2.2×10^{-5}	1.2464
[8/6; 4]	-0.1715700	1.7×10^{-5}	1.2476
[8/6; 5]	-0.1715621	6.3×10^{-5}	1.2310
[9/4; 2]	-0.1715693	2.1×10^{-5}	1.2472
[9/4; 3]	-0.1715676	3.1×10^{-5}	1.2467
[9/4; 4]	-0.1715684	2.6×10^{-5}	1.2466
[9/4; 5]	-0.1715692	2.2×10^{-5}	1.2471
[9/4; 6]	-0.1715572	9.1×10^{-5}	1.2152
[9/5; 3]	-0.1715658	4.1×10^{-5}	1.2458
[9/5; 4]	-0.1715691	2.2×10^{-5}	1.2469
[9/5; 5]	-0.1715690	2.3×10^{-5}	1.2460
[9/6; 4]	-0.1715709	1.1×10^{-5}	1.2483
[10/4; 2]	-0.1715630	5.7×10^{-5}	1.2448
[10/4; 3]	-0.1715686	2.5×10^{-5}	1.2470
[10/4; 4]	-0.1715681	2.8×10^{-5}	1.2457
[10/4; 5]	-0.1715643	5.0×10^{-5}	1.2385
[10/5; 3]	-0.1715698	1.8×10^{-5}	1.2476
[11/4; 2]	-0.1715688	2.4×10^{-5}	1.2471
[11/4; 3]	-0.1715692	2.2×10^{-5}	1.2473
[11/4; 4]	-0.1715669	3.5×10^{-5}	1.2433
[11/5; 3]	-0.1715707	1.2×10^{-5}	1.2481

Table 14: Continuation of DA Table for u_e Singularity.

Figure Caption

Fig. 1. Assignment of couplings K_i , $i = 1, 2, 3, 4$ to links (bonds) of the checkerboard lattice.

Fig. 2. (a) Phases and associated boundaries in the complex u plane for the Ising model on the square lattice with $h = \pm i\pi/2$. The boundaries are given by eqs. (2.32) and (2.33) in the text. In particular, the line segment extends from u_e as given in eq. (2.34) off the figure to the left, ending at $1/u_e = -(3 + 2\sqrt{2}) \simeq -5.828$. FM and AFM refer to phases in which $M \neq 0$, $M_{st} = 0$ and $M = 0$, $M_{st} \neq 0$, respectively. (b) Complex-temperature phase diagram in the v plane.

Fig. 3. Path of κ^2 corresponding to $u = \rho e^{i\theta}$ for $\theta = \pi/6$, as ρ varies from 0 to 30. Horizontal and vertical axes are the $Re(\kappa^2)$ and $Im(\kappa^2)$ axes. The image of the singular curve (2.32) and line segment (2.33) is the dark line from $\kappa^2 = 1$ to $\kappa^2 = \infty$.

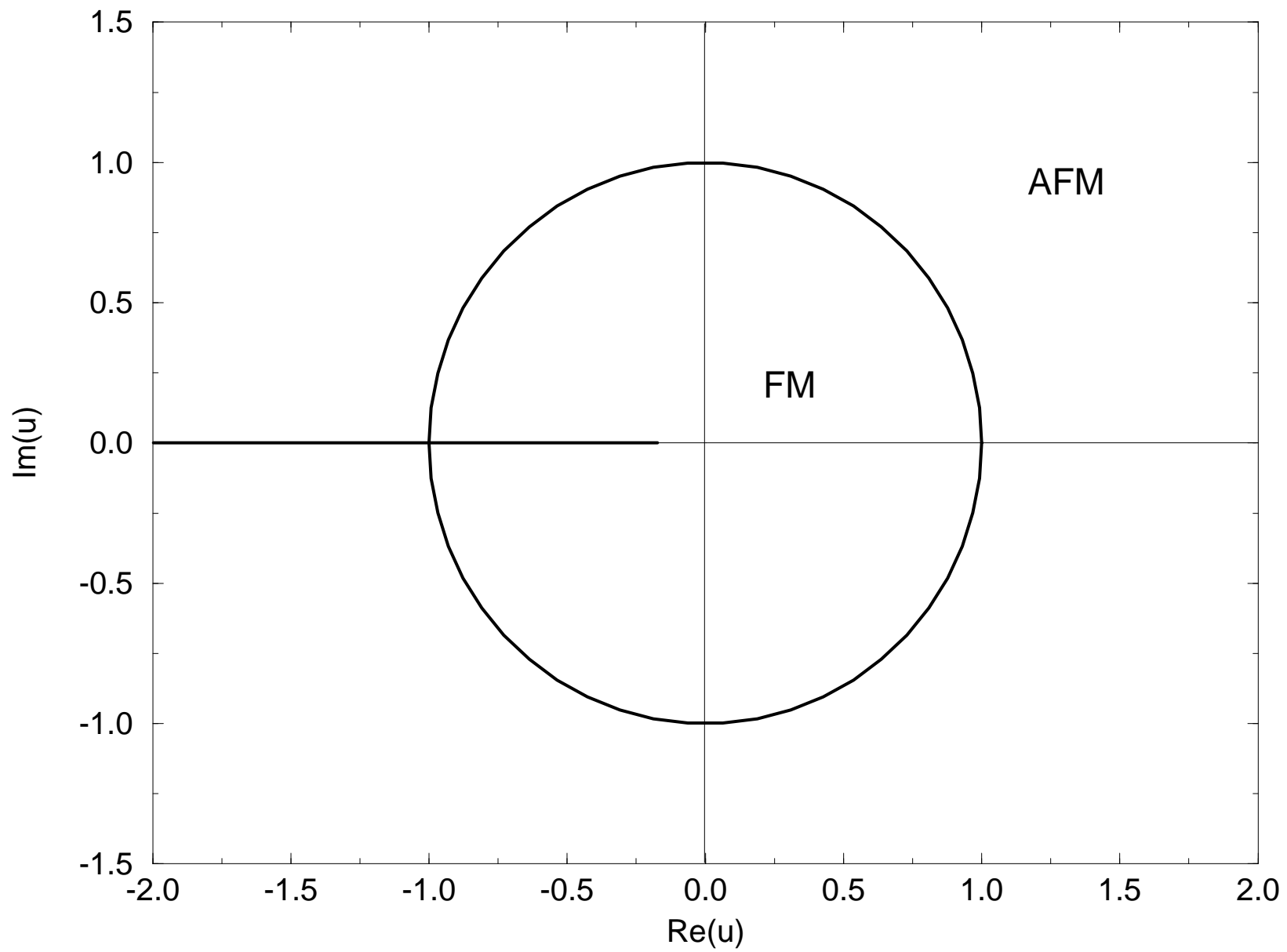
This figure "fig1-1.png" is available in "png" format from:

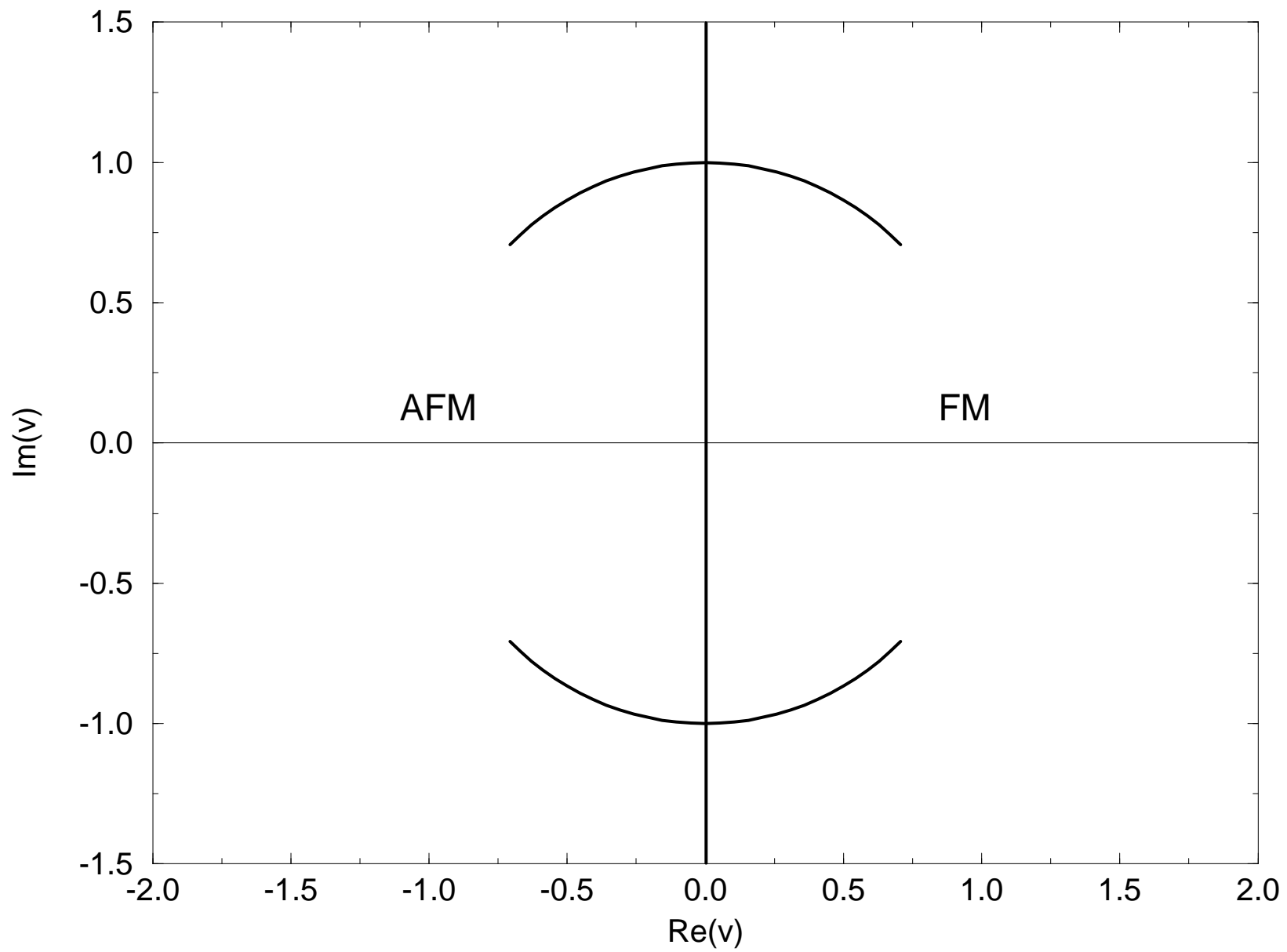
<http://arxiv.org/ps/hep-lat/9412105v1>

	K_1	K_3	
K_4		K_2	K_4
	K_3	K_1	
K_2		K_4	K_2
	K_1	K_3	

This figure "fig1-2.png" is available in "png" format from:

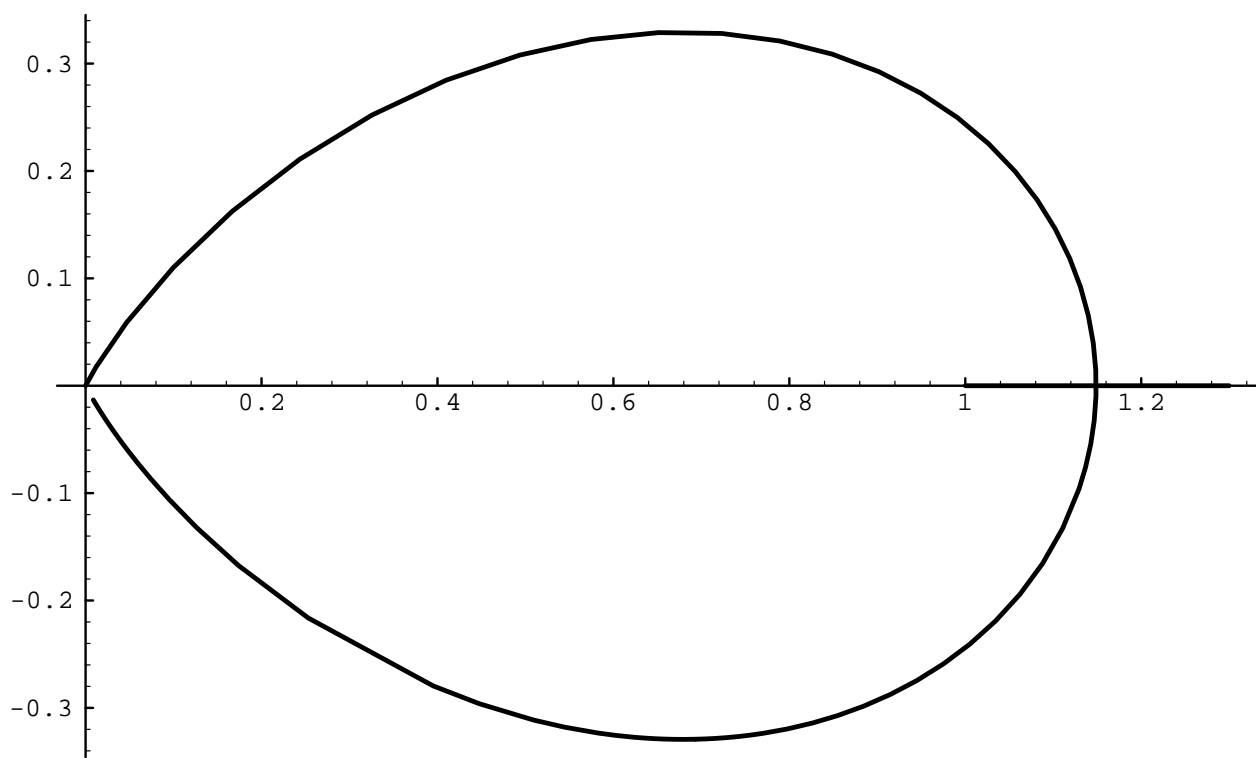
<http://arxiv.org/ps/hep-lat/9412105v1>





This figure "fig1-3.png" is available in "png" format from:

<http://arxiv.org/ps/hep-lat/9412105v1>



This figure "fig1-4.png" is available in "png" format from:

<http://arxiv.org/ps/hep-lat/9412105v1>